Principles of checkpoint override

Ahmad SADEGHI

Acceptée sur proposition du jury

Prof. F. Courbin, président du jury
Prof. S. J. Rahi, directeur de thèse
Prof. S. Martin, rapporteuse
Prof. N. Buchler, rapporteur
Dr A. Verkhovsky, rapporteur

To my parents and my forever love, Zahra.

Acknowledgements

Abstract

Quality-control and surveillance systems are critical for biological systems. In particular, the cell cycle, which is the process by which cells replicate, is controlled by multiple checkpoint systems, which arrest cells when certain conditions are not met. Checkpoints ensure that requirements on nutrient levels, genome integrity, and attachment of chromosomes to the spindle, the machinery that pulls genetic material into two daughter cell, are fulfilled before cells can pass specific transitions in the cell cycle. However, many of these quality-control systems fail or are overridden: After prolonged arrests, the cell cycle continues despite the presence of errors.[1–6] The reasons for checkpoint override have remained mysterious. In particular, checkpoint override is not understood quantitatively by experiment or theory. This is the knowledge gap that I sought to fill with my thesis work. I sought to find dynamical laws obeyed by error-correction and quality-control systems, using DNA repair and the DNA damage checkpoint in budding yeast as specific experimental models. First, I helped derive a general theory of optimal checkpoint strategies, balancing the trade-off[7,8] between risk and self-replication opportunity. We demonstrated that the mathematical problem of finding the optimal strategy maps onto the question of calculating the optimal absorbing boundary for a random walk, which we showed can be solved efficiently recursively. The theory predicted the optimal override time without free parameters based on the statistics i) of error correction and ii) of survival. We applied the theory experimentally to the DNA damage checkpoint in budding yeast. We built budding yeast strains, in which we could control the cell cycle stage, introduce a precise number of DNA breaks, and monitor DNA repair and checkpoint override. For this, we developed a DNA break sensor whose fluorescence signal changed depending on whether a DNA break was present or not. Using these systems, we quantified i) the probability distribution of repair for a double-strand DNA break (DSB), including for the critically important, rare events deep in the tail of the distribution and ii) the survival probability after

Abstract

override. Based on these parameters, the theory predicted the theoretically optimal DNA damage override times. Finally, we measured these times precisely experimentally. We found a remarkably close match between the optimal theory and measurements of the DNA damage checkpoint override times as a function of the number of DSBs. The universal nature of the balance between risk and self-replication opportunity is in principle relevant to many other systems, suggesting potential further applications of the theory.

Keywords: Cell cycle, checkpoint, DNA damage, DNA break, override, adaptation, slippage, budding yeast, fitness

Résumé

Les systèmes de contrôle de la qualité et de surveillance sont essentiels pour les systèmes biologiques. En particulier, le cycle cellulaire, qui est le processus par lequel les cellules se répliquent, est contrôlé par de multiples systèmes de points de contrôle, qui arrêtent les cellules lorsque certaines conditions ne sont pas remplies. Les points de contrôle garantissent que les exigences relatives aux niveaux de nutriments, à l'intégrité du génome et à l'attachement des chromosomes au fuseau, la machinerie qui entraîne le matériel génétique dans deux cellules filles, sont remplies avant que les cellules puissent passer à des transitions spécifiques dans le cycle cellulaire. Cependant, bon nombre de ces systèmes de contrôle de la qualité échouent ou sont dépassés : Après des arrêts prolongés, le cycle cellulaire se poursuit malgré la présence d'erreurs.[1–6] Les raisons de ce contournement des points de contrôle sont restées mystérieuses. En particulier, le dépassement des points de contrôle n'est pas compris quantitativement par l'expérience ou la théorie. C'est ce manque de connaissances que j'ai cherché à combler avec mon travail de thèse. J'ai cherché à trouver des lois dynamiques auxquelles obéissent les systèmes de correction des erreurs et de contrôle de la qualité, en utilisant la réparation de l'ADN et le point de contrôle des dommages à l'ADN chez la levure *Saccharomyces cerevisiae* comme modèles expérimentaux spécifiques. Tout d'abord, j'ai aidé à dériver une théorie générale des stratégies optimales de point de contrôle, en équilibrant le compromis[7,8] entre le risque et l'opportunité d'auto-réplication. Nous avons démontré que le problème mathématique consistant à trouver la stratégie optimale correspond à la question du calcul de la limite d'absorption optimale pour une marche aléatoire, dont nous avons montré qu'elle pouvait être résolue efficacement de manière récursive. La théorie a prédit le temps optimal d'absorption sans paramètres libres en se basant sur les statistiques i) de la correction des erreurs et ii) de la survie. Nous avons appliqué la théorie expérimentalement au point de contrôle des dommages à l'ADN chez la levure *S. cerevisiae*. Nous avons construit

des souches de levure *S. cerevisiae* dans lesquelles nous pouvions contrôler le stade du cycle cellulaire, introduire un nombre précis de cassures de l'ADN et surveiller la réparation de l'ADN et le dépassement du point de contrôle. Pour cela, nous avons développé un capteur de cassure d'ADN, dont le signal de fluorescence change selon qu'une cassure d'ADN est présente ou non. À l'aide de ces systèmes, nous avons quantifié i) la distribution de probabilité de réparation d'une cassure double brin de l'ADN (CDB), y compris pour les événements rares d'importance critique situés dans la queue de la distribution, et ii) la probabilité de survie après le dépassement du point de contrôle. Sur la base de ces paramètres, la théorie a prédit les temps de dépassement des dommages à l'ADN théoriquement optimaux. Enfin, nous avons mesuré ces temps avec précision de manière expérimentale. Nous avons trouvé une correspondance remarquablement étroite entre la théorie optimale et les mesures des temps de dépassement du point de contrôle des dommages à l'ADN en fonction du nombre de CDB. La nature universelle de l'équilibre entre le risque et l'opportunité d'auto-réplication est en principe pertinente pour de nombreux autres systèmes, ce qui suggère d'autres applications potentielles de la théorie.

Mots clés : Cycle cellulaire, point de contrôle, dommages à l'ADN, cassure de l'ADN, dépassement, adaptation, levure *S. cerevisiae*, fitness.

Contents

Contents

List of Figures

List of Tables

Abbreviations

dsDNA   double-strand DNA

DDC   DNA damage checkpoint

DSB   double-strand DNA break

FACS   fluorescence-activated cell sorting

HR   homologous recombination

Met   methionine

MMEJ   microhomology-mediated end joining

NHEJ   non-homologous end joining

ODE   ordinary differential equation

ssDNA   single-strand DNA

SAC   spindle assembly checkpoint

YFP   yellow fluorescent protein

1 Introduction

1.1 Quantitative approaches to checkpoint override

Checkpoints are molecular systems that ensure the self-replication cycle of cells, the cell cycle, progresses only when certain criteria are met.[9] Checkpoint function is critical for health, and dysfunction contributes to numerous diseases, including cancer.[6,10–14] Checkpoints consist of complex gene networks and are dynamic: They turn on, off, and some checkpoints are known to override (adapt) despite persistent damage. Checkpoint override has been observed in yeast[1,2,6,15] and mammals[3,5,16] in the DNA damage checkpoint (DDC), the spindle assembly checkpoint (SAC), and for developmental checkpoints[4,17,18].

Although checkpoint override has been researched for decades,[3,5,16] a system-level, quantitative, and dynamic analysis of checkpoint override did not exist. A goal of my thesis work was to begin to explore checkpoints from this perspective.

1.2 Double-strand break (DSB) repair

Double-strand DNA breaks (DSBs) can be caused by a variety of processes including DNA replication, mitotic forces, or radiation and chemicals in the environment.[6,10–14] Improper repair of DSBs can lead to genomic instability, which is why DSB repair has been intensely researched, and budding yeast has served as a major model for elucidating DSB repair processes[6].

1

Three types of DSB repair are generally distinguished: non-homologous end joining (NHEJ), homologous recombination (HR), and microhomology-mediated end joining (MMEJ).[6,13] NHEJ usually leads to a simple religation of the DNA ends generated by a break. NHEJ, however, can also religate DNA unfaithfully, generating mutations at the break site. If religation does not occur rapidly, the DNA is resected, that is, nucleotides are removed from one of the DNA strands in the 5' to the 3' direction, exposing single-strand DNA (ssDNA) and a 3' overhang. This ssDNA is the prerequisite for both MMEJ and HR. HR requires a homologous template elsewhere in the genome, which exists, for example, in diploid cells on the second homologous chromosome. In HR, the ssDNA is used to find the homologous template, which is used for repairing the break. The different repair pathways are controlled by different genes. HR requires the resection machinery and *RAD52*, MMEJ in addition requires *RAD1-RAD10*, and NHEJ requires *YKU70* and *YKU80*. While NHEJ can occur throughout the cycle, it is the main repair pathway in G1 phase.

The first step in these repair processes is the recognition of the ends of broken chromosomes by the Mre11-Rad50-Xrs2 complex (MRX or MRN in mammals). The next step is the recruitment of Tel1 kinase. The sliding clamp complex (called the 9-1-1 complex, formed of Ddc1, Rad17, and Mec3 in budding yeast) then binds the dsDNA-ssDNA junction, and RPA binds to ssDNA and recruits the Mec1-Ddc2 dimer. Mec1 and Tel1 go on to activate the DNA damage checkpoint, which arrests the cell cycle, and to activate repair.

1.3 DSB repair kinetics

Measuring repair kinetics is critical for gaining a quantitative understanding of DNA repair and the DNA damage checkpoint. However, NHEJ, for example, had primarily been measured in bulk culture and only with relatively low temporal resolution. Measurements have traditionally been performed using qPCR[19–22] or other bulk culture methods[23]. The measurements have generally been too coarse to deduce typical timescales for repair, e.g., $\approx$50% repair was seen in about 6 hrs[22].

An alternative approach has been to aim to detect DSBs with fluorescently tagged proteins which bind near DSBs.[24–26] However, the reliability of foci formation is difficult to estab-

lish[24,26]. Furthermore, the fluorescent signals are too weak to be detectable by flow cytometry, which is needed to analyze large numbers of cells for rare events.

1.4 DNA damage checkpoint (DDC): activation and override

The DNA damage checkpoint causes delays in the cell cycle during which repair can occur.[6,10–14] The DDC acts at three different stages, at the G1/S transition, during S phase, and at the G2/M transition.

The first step in DDC activation is the binding of the MRX complex at the DNA ends. Tel1 is then recruited, followed by Sae2, Exo1, Dna2-Sgs1, and resection of DNA. After RPA coats ssDNA, the Mec1-Ddc2 dimer is recruited to the DNA, and Dpb11 and the 9-1-1 (Ddc1-Rad17-Mec3) complex activate Mec1. The Mec1-Ddc2 dimer and Tel1 then phosphorylate and activate the central checkpoint kinase Rad53 with Rad9 serving as a mediator in this process. Rad53 is a central hub in the DNA damage checkpoint, which integrates the signals from Mec1 and Tel1. The checkpoint blocks anaphase in part by active Rad53 preventing APC-Cdc20 function. Rad53 dephosphorylation coincides with a downregulation of the DDC, and is often taken to be the key determinant of checkpoint downregulation.

In budding yeast, a single unrepaired DSB activates the DDC, yet, after ≈8 hr arrest at the G2/M checkpoint, cells proceed with the cell cycle although the DSB is not repaired.[1,2,27] This coincides with the dephosphorylation of Rad53, and the phenomenon has been termed checkpoint adaptation or override. DNA damage due to X-rays[28] or telomere dysfunction[2,29] also lead to checkpoint override. A number of mutations have been found to prevent or reduce checkpoint override, notably *cdc5-ad* (missense mutation in *CDC5*)[2], *ckb2Δ*[2], *yku70Δ*[27], among others discussed below[30,31].

The existence of mutations that abrogate override underscores the possibility that DNA damage checkpoint override is functionally important to yeast cells. However, past work had not shown definitively that override has a benefit for wild-type cells nor explained the importance of its timing (≈8 hrs after one DSB). A key test to establish whether override has a functional role is whether cells with DNA damage produce more offspring on average, if they override their checkpoint. This was found not to be the case; in haploid yeast cells, no

significant difference was found between survival rates of override-competent (*CDC5*) or override-incompetent (*cdc5-ad*) cells after X-ray irradiation.[28] On the other hand, a situation in which checkpoint override was beneficial was created experimentally by blocking critical pathways for DNA repair (*rad52Δ*) or telomere maintenance (*tlc1Δ*).[28,32,33] (This is likely to be relevant since checkpoint override occurs in cancer cells that often have lost one or another DNA repair mechanism.) Furthermore, it was found that DNA damage checkpoint override occurred only if exactly one endonuclease-generated DSB was present but not if the cell had two DSBs[27].

Many genes have been shown to affect checkpoint override, including *CDC5*[2], *RAD53*[34], *PTC2*[30,35], *PTC3*[30,35], *MEC1*[36], *DDC2*[36], *YKU70*[27], *MRE11*[27], *RAD51*[37], *SRS2*[32], *SAE2*[38], *RDH54*[39], *YKU70*[27], *EXO1*[40], *FUN30*[40], *VPS51*[41], *YPT6*[41], *CMR1*[42], *RPD3*[42], *BTN2*[42], and *HSP42*[42]. How this large network computes the decision to override is mostly not understood. However, a core network involving (*CDC5*, *RAD53*, *MEC1*, *DDC2*, and the protein phosphatase *PTC2* or its paralog *PTC3*) is widely considered to be key.[6,43] A second phosphatase, Pph3[43–45], is sometimes considered to be important for DDC override but a *pph3Δ* deletion was not sufficient to delay DDC override.[44] The DDC network is particularly challenging to study because reversible phosphorylation events are critical for its establishment, maintenance, and reversal.
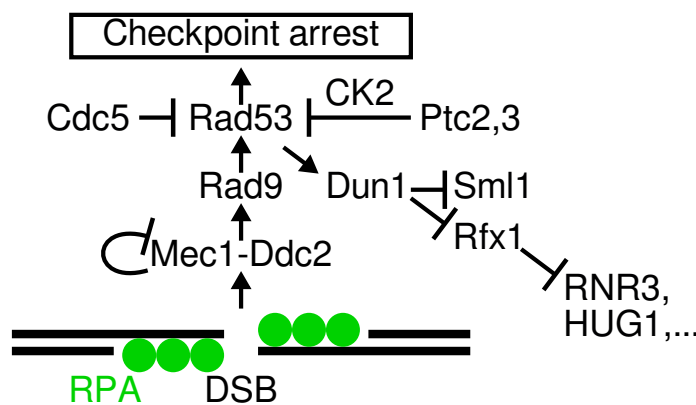
Fig. 1.1 – Core wiring diagram for DDC override.

The *cdc5-ad* mutation of the Polo-like kinase *CDC5* was one of the first to be found to prevent checkpoint override.[2] Cdc5 is controlled transcriptionally as well as post-transcriptionally. Since transcriptional activation of *CDC5* using the *GAL1* promoter sufficed to speed up check-

point override, we conclude that transcriptional induction during checkpoint arrest may suffice for Cdc5 activity.[46,47] This result also indicated that the *cdc5-ad* mutation could plausibly be a loss-of-function mutation. However, it was found that phosphorylation of Rad53 by Cdc5 was needed for DDC override[48], suggesting that *cdc5-ad* was a gain-of-function mutation. Thus, the role of Cdc5 has remained difficult to pin down.[49]

The PP2C phosphatases Ptc2 and Ptc3 dephosphorylate Rad53, thereby silencing it and allowing override.[30] Ptc2 is thought to be controlled post-translationally by another kinase, casein kinase 2 (CK2) to perform this function.[35] However, Ptc2 activity may not be strongly regulated and represent a constitutive phosphatase activity.[35] Consistently, the transcripts of *PTC2* and *PTC3* are not upregulated with DNA damage.[50]

The amount or rate of resected DNA was thought to determine the timing of DDC override.[27,31] However, newer data called this model into question: Some mutations that slow down resection (*sgs1Δ*, *fun30Δ*) block override and certain mutations that increase resection (*H2BK123*) speed up override.[6]

1.5   Importance of DDC override

Elucidating checkpoint override from a quantitative perspective can also be expected to advance our understanding of disease. Checkpoints are corrupted in many diseases that are driven by genetic alteration.[6,10–14] Checkpoint override is associated with genomic instability and aneuploidy in yeast and mammalian cells,[3,16,28,29,33,51] and with cancer emergence or exacerbation in human cells.[5] Tumor-derived U2OS cells arrest in response to ionizing irradiation and then override the DDC.[16]

Checkpoint override provides growth advantages to yeast cells with one double-strand DNA break (DSB), as I showed in my thesis work.[52] Thus, it is reasonable to speculate that cancer cells explore checkpoint override as a growth strategy and remodel the checkpoint toward increased cellular fitness[53]. Future exploration of this subject in budding yeast should intensify interest in such questions.

Checkpoint override also occurs in entirely different systems. In response to injury, check-

points arrest insect development, and some of these checkpoints have been shown to be overridden if the damage is not repaired.[4] *Drosophila* larvae delay but do not block entry into pupariation if their imaginal discs are damaged at specific developmental stages.[17] Principles (but not molecular mechanisms) gleaned from yeast may feed into the broader research efforts into checkpoints.

1.6   Biophysics can help elucidate checkpoints

Checkpoints are subjects of intense current interest due to their biological and medical importance. However, checkpoints are also conceptually fascinating for biophysicists. Checkpoints create a risk-speed trade-off: Whenever self-replication arrests because of errors, opportunities for producing offspring decrease as a consequence of the delay.

Fig. 1.2 – Hypothetical balance setting checkpoint override times.

On the other hand, delays may be necessary for correcting errors, e.g., for DNA damage repair.[54] How this balance (Fig. 1.2) may have shaped checkpoints and their ability to be overridden is not understood.

In addition to being conceptually interesting, the checkpoint network is well suited to taking a biophysical approach because many of the fundamental open questions in the field require quantitative, single-cell measurements. However, biophysics has contributed less to checkpoint studies than to many other fields.

1.7   Past theoretical work

1.7.1   System-level theories

Despite the importance of checkpoints to biology, a theoretical understanding of checkpoint trade-offs or strategies had not been developed. While researchers have pointed out that checkpoints may balance opposing demands on repair success and speed,[27,28,32,33] these ideas had not been developed into a quantitative theory of checkpoint strategies. This is precisely the gap I began to fill by providing a system-level description of checkpoint strategies

in terms of error repair probabilities, survival probabilities, and checkpoint arrest durations depending on the amount of DNA damage. The balances that checkpoints strike are different from speed-accuracy-energy dissipation balances or decision-making frameworks proposed for sensing in chemotaxis or kinetic proofreading.[7,55–70] For checkpoints, errors such as DNA damage or poor chromosome-spindle attachment are thought to be signaled reliably,[71] and uncertainty arises from the stochastic nature of the outcomes (survival, sickness, or death).

More closely related to our approach are analyses of the benefits of DNA repair to cancer cells, based on coarse-grained parameters.[72–74] While these ideas bear similarities to ours, quantitative predictions and validation are rare.

1.7.2 Chemical kinetics models

In contrast to analyses of checkpoint strategies, a number of chemical kinetic models describing the dynamics of the molecular components of checkpoints have been published. Checkpoint activation has been modeled by systems of ordinary differential equations (ODEs) for yeast[75,76] or mammalian cells[77–86], which were in part followed up by experimental tests[76,85].

As far as our literature searches revealed, DDC override has not been modeled before, even though it emerges as a decision of a complex network, which requires modeling for a clear understanding of the mechanism. (Override of the spindle assembly checkpoint has, however, been modeled, and we will consider stochastic escape as a possible mechanism.[76]) Biochemical kinetics models have been very successful at describing the cell cycle oscillator.[87] In many cases, models are proposed based on a consensus wiring diagram of gene interactions, which is turned into an ODE model by 'educated guesses'.[87]

2 Optimal checkpoint strategies

This chapter is based on a paper currently in review:

I helped conceptualize this research project, carried out the experiments, helped advance the theory and helped write the manuscript.

2.1   Abstract

Why biological quality-control systems fail is often mysterious. Specifically, checkpoints in yeast and animals are overridden after prolonged arrests allowing self-replication to proceed despite the continued presence of errors.[1–6] Although critical for the organism, checkpoint override is not understood quantitatively by experiment or theory. To uncover dynamical laws obeyed by error-correction systems, we derived a general theory of optimal checkpoint strategies, balancing the trade-off[7,8] between risk and self-replication opportunity. We demonstrate that the mathematical problem of finding the optimal strategy maps onto the question of calculating the optimal absorbing boundary for a random walk, which we show can be solved efficiently recursively. The theory predicts the optimal override time without free parameters based on the statistics i) of error correction and ii) of survival. We applied the theory experimentally to the DNA damage checkpoint in budding yeast, an intensively researched model for eukaryotic checkpoints, whose override is nevertheless not understood quantitatively, functionally, or at the system level. Using a novel fluorescent construct which allowed cells with DNA breaks to be isolated by flow cytometry, we quantified i) the probability distribution of repair for a double-strand DNA break (DSB), including for the critically important, rare events deep in the tail of the distribution and ii) the survival probability after override. Based on these two measurements, the optimal checkpoint theory predicted remarkably accurately the DNA damage checkpoint override times as a function of DSB numbers, which we also measured for the first time precisely. Thus, a first-principles calculation uncovered hitherto hidden patterns underlying the highly noisy checkpoint override process. Our multi-DSB results revise well-known bulk culture measurements[27] and show that override is a more general phenomenon than previously thought. The universal nature of the balance between risk and self-replication opportunity is in principle relevant to many other systems, suggesting potential further applications[4,74].

2.2 Introduction

Error detection and correction during self-replication processes are subjects of intense current interest. However, fundamental questions remain unanswered. A risk-speed trade-off emerges by necessity in biological surveillance systems: Whenever self-replication arrests because of errors, opportunities for producing offspring decrease as a consequence of the delay. On the other hand, delays may be necessary for correcting errors, e.g., for DNA damage repair.[54] How this simple idea can lead to the potential discovery of quantitative, system-level patterns obeyed by biological surveillance systems has remained unexplored.

Cell cycle checkpoints arrest the self-replication process, thus limiting its speed, and increase the chances of survival when a cell encounters errors.[6,71,88] However, checkpoints show more complex behaviors than merely gating the cell cycle depending on the presence or absence of errors. After prolonged arrests, checkpoints such as the DNA damage checkpoint or the spindle assembly checkpoint (SAC) are overridden in the continued presence of errors, which is associated with genomic instability and aneuploidy in yeast and mammalian cells.[3,16,28,29,33,51] (We opt for the more general term 'override' in place of 'adaptation', 'slippage', or 'leakage'[3].)

Despite the importance of checkpoints to living systems, there are no quantitative theories of checkpoint trade-offs or strategies. Many researchers have pointed out that checkpoints may balance opposing demands on repair success and speed.[27,28,32,33] However, these ideas have so far not been developed into a quantitative theory of checkpoint strategies, which would motivate experimental measurements of the parameters of the theory and lead to validation of new predictions. Chemical kinetic models represent the dynamics of the molecular components of checkpoints[76,77,83] but they do not indicate potential strategies for checkpoints in an obvious manner as they primarily describe the state of the system in time. Similarly, the potential balances that checkpoints strike are not straightforwardly explained by speed-accuracy-energy dissipation relations or decision-making frameworks proposed for other systems: Sensing in chemotaxis and mechanisms for kinetic proofreading address the difficulties of ascertaining information and decision-making in the presence of noise.[7,55–70] This contrasts with the case of checkpoints where errors such as DNA damage or poor chromosome-spindle attachment are signaled reliably;[71] uncertainty arises from the seemingly stochastic

nature of the outcomes (survival, sickness, or death).

Experiments support the existence of a balance between risk and speed qualitatively: Budding yeast cells with dysfunctional DNA damage (*rad9Δ*) or spindle assembly checkpoints (*mad2Δ*), which arrest very briefly[6] or not noticeably[71], die at much higher rates in the presence of DNA damage or poor spindle-chromosome binding.[71] Multiple experimental challenges have to be overcome in order to resolve checkpoint strategies more quantitatively:

- The differences between strategies may manifest in rare events, which, by their nature, are difficult to capture experimentally, e.g., rare, late repair events. (Over evolutionary timescales or in large populations, rare beneficial outcomes can nevertheless suffice for selection and fixation.)

- Checkpoints and repair systems are complicated, involving many different genes and pathways, which makes it difficult to isolate and study specific effects without confounding factors.

The DNA damage checkpoint in budding yeast, which has been intensively studied by molecular biology and genetics,[6,71] is particularly ripe for quantitative, system-level insights. In haploid cells, which cannot utilize highly efficient template-based DNA repair mechanisms such as homologous recombination, DSBs remain unrepaired in a substantial fraction of cells for many hours.[89] For a single unrepaired DSB near the left telomere of chromosome VII, the MAT locus, or *URA3*, it was observed that after an ≈8 hr arrest at the G2/M checkpoint, cells proceeded with the cell cycle although the DSB was not repaired.[1,2,27] Difficult-to-quantify but possibly large amounts of DNA damage due to X-rays[28] or telomere dysfunction[2,29] also lead to checkpoint override. A number of mutations have been found to prevent or reduce checkpoint override: *cdc5-ad* (missense mutation in *CDC5*)[2], *ckb2Δ*[2], *yku70Δ*[27], and others[30,31].

The existence of mutations that abrogate override underscores the possibility that DNA damage checkpoint override is functionally important to yeast cells. However, past work has not shown that override has a benefit for wild-type cells nor explained the importance of its timing (≈8 hrs): A key test to establish whether override has a functional role at all is whether cells with DNA damage produce more offspring on average if they override their checkpoint. This was

found not to be the case; in haploid yeast cells, no significant difference was found between survival rates of override-performing (*CDC5*) or override-unable (*cdc5-ad*) cells after X-ray irradiation, which causes DSBs.[28] (A situation in which checkpoint override was beneficial was created by artificially blocking critical pathways for DNA repair (*rad52Δ*) or telomere maintenance (*tlc1Δ*).[28,32,33]) Furthermore, it was found that DNA damage checkpoint override occurred only if exactly one endonuclease-generated DSB was present but not with two DSBs[27], indicating that override happens only under specific conditions and is not a universal response to DNA damage in yeast. Thus, the functional relevance of override remains unclear.

A quantitative analysis of checkpoint strategies requires the statistics of rare repair events, which have not been measured. In the absence of a genomic template with a similar DNA sequence, repair occurs by non-homologous end joining (NHEJ)[90], whose timing and efficiency after DSB induction has been measured, for example, by performing qPCR[19–22] or other quantification methods[23] in bulk culture at regular time points after the break event. These measurements showed broadly distributed repair times such that a typical repair timescale could not be easily deduced ($\approx$50% repair in about 6 hrs[22]). Bulk culture assays may be too insensitive to quantify rare and late repair events.

Here, we present

1. the first, general theory of optimal checkpoint strategies, which is based on the fundamental principle of offspring maximization,

2. measurements of the two parameters of the theory, the probability distribution function of repair and the survival probability after checkpoint override,

3. predictions of the theory: optimal override times as a function of the numbers of DSBs,

4. quantitative experimental verification of the predictions, and

5. the first measurements showing that override is indeed advantageous with wild-type DNA repair machinery.

2.3 Results

2.3.1 Theoretical results

Arrest implies an exponential fitness penalty

To compute the fitness effects of different checkpoint strategies, we compared an arrested cell to other cells in the population theoretically. The two canonical scenarios of population genetics are exponential growth (Fig. 2.1 A) and stochastic birth-death processes in a fixed-size population (Fig. 2.1 B).[91]

In exponential growth, the expected number of progeny of a checkpoint-arrested cell is reduced by $2^{-t/T}(P_2 + P_1/2)$, where t is the arrest time, P_2 the probability that both progeny proliferate after the arrest, and P_1 the probability that only one progeny proliferates (Fig. 2.1 A). (In this presentation, cells either die or produce healthy progeny, in agreement with experimental observations, see Supplementary Information.)

We also analyzed the effect of checkpoint arrest on the expected number of progeny in two classical fixed-size population models, the Wright-Fisher and the Moran models[91] (Supplementary Information). Here, the reduction in the expected number of progeny has the same form as for exponential growth: the product of a penalty for the arrest time, which is exponential, multiplied by a probability of proliferation. Thus, one can represent the arrest penalty by a general factor $e^{-t/\tau}$, which applies in all three cases and where τ absorbs model-specific parameters, for example, $\tau = T/\log 2$ for exponential growth.

Winning strategy maximizes the arithmetic mean of the future progeny

To evaluate how different strategies influence an organism's reproductive success, one of two quantities is commonly taken as a fitness function, i) the number of offspring averaged over all possible outcomes or ii) the expected number of offspring in a typical scenario.[7,91,92] In some instances, such as in fluctuating environments, the typical series of outcomes (ii) is thought to be the more relevant quantity for evolutionary selection[91,92], favoring bet hedging[93]. However, since errors and checkpoint arrests affect cells randomly, averaging over the predicted
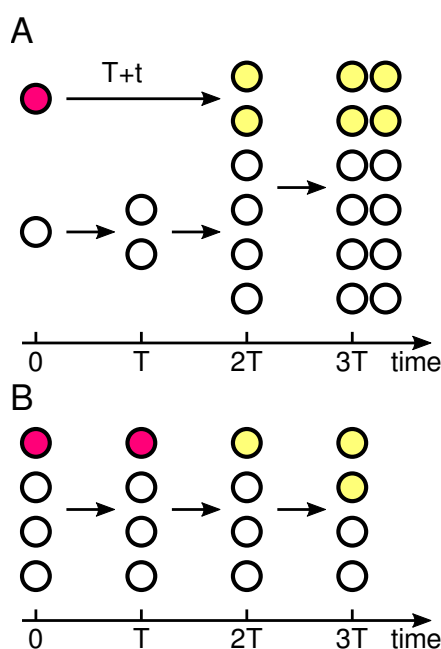
Fig. 2.1 – Scenarios for the self-replication dynamics of a checkpoint-arrested cell (magenta circle) in a population of cells (white) with generation time T. A: The exponential growth with doubling time T is delayed by a checkpoint arrest of duration t (= T in this illustration) after which both, one, or no progeny (yellow circles) remains viable. Only the case where both progeny are viable is illustrated. B: In a population of fixed size N, random birth-death processes change the proportions of different clones, as in the Wright-Fisher or Moran models.

number of offspring (i) is the appropriate fitness function to consider here, as we illustrate by contrasting a random checkpoint arrest model with a fluctuating-environment model in the Supplementary Information.

Checkpoint strategy parameters

In addition to the arrest penalty, an experimentally accessible set of parameters for analyzing checkpoint strategies are needed:

- The remaining number of *e*rrors $E(t)$ in a cell after arresting for time t, for example, DSBs (potentially signaled by the amount of RPA covering resected DNA) or unattached kinetochores. $E_0 = E(0)$ denotes the initial number of errors, and $E(t)$ decreases with the arrest time t as errors are corrected.

- The probability $r(\{t_i\})$ that the errors are *r*epaired at times $\{t_i\} = \{t_1, \ldots, t_{E_0}\}$. When needed, we will assume that each error is repaired independently with the cumulative

15

probability density function $\rho(t)$ for the repair of a single error.

- The probability $s(t|\{t_i\})$ of **s**urvival if a checkpoint is overridden after an arrest of duration t given that repairs take place at times $\{t_i\}$. (A repair time t_i after t ($t_i > t$) indicates that error i was not fixed before the checkpoint is overridden.) To simplify, we will just write $s(E)$ when the survival probability only depends on the number of remaining errors $E(t)$. If each error reduces the survival probability by the same amount, we will write $s(E) = \sigma^E$.

- The probability of cell cycle **a**dvancement $a(t|\{t_i\})$, that is, of override if there are unrepaired errors or of continuation of the self-replication cycle if there are no errors. The cell cycle advancement probability $a(t|\{t_i\})$ represents the checkpoint strategy and is the function that we seek to compute.

$E(t)$, $r(t|\{t_i\})$, and $s(t|\{t_i\})$ represent the state of the cell and are determined by biochemical processes. The function $a(t|\{t_i\})$ represents the behavior of the checkpoint whose effect on the reproductive success of the cell we analyze.

General mathematical description of checkpoint strategies

Combining the above probabilities, the fitness coefficient f is the factor by which the number of progeny is changed due to the damage and the subsequent behavior of the checkpoint:

$$f[a] = \int_0^\infty dt \prod_{E=1}^{E_0} dt_E\, r(\{t_i\})\, s(t|\{t_i\})\, a(t|\{t_i\})\, e^{-t/\tau} \quad . \tag{2.1}$$

Additional information regarding this expression is given in the Supplementary Information.

To visualize the processes that this functional represents, we make two simplifications: each repair occurs independently and each error reduces the survival probability by the same amount. This allows a graphical interpretation of the mathematical expressions, depicted in Fig. 2.2 A.
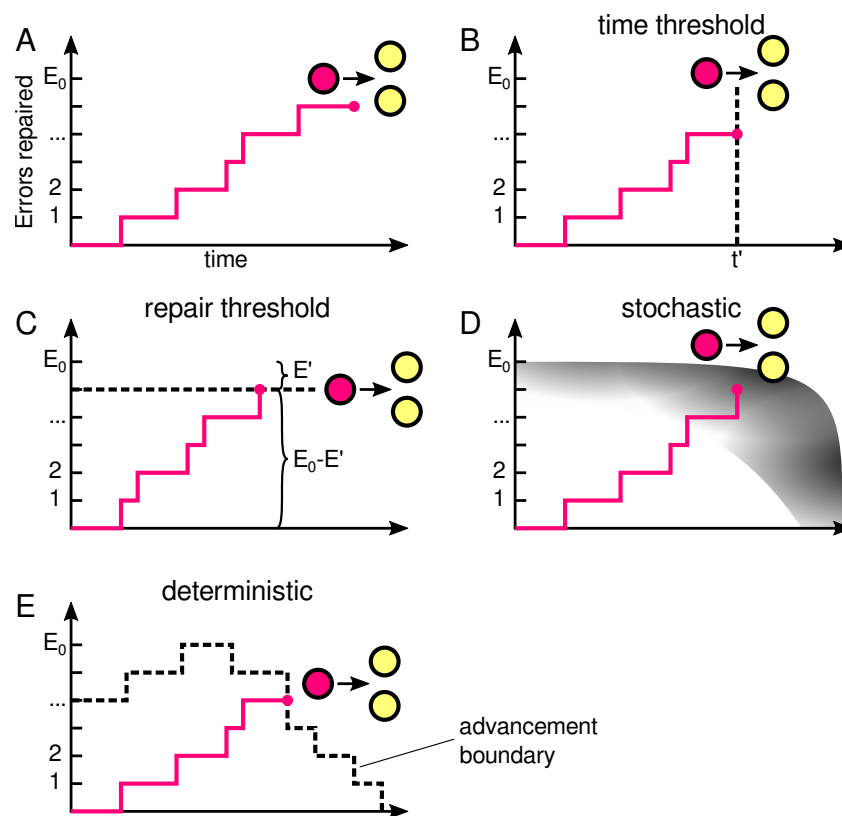
Fig. 2.2 – Pictorial representation of checkpoint strategies. A: A checkpoint-arrested cell (red) moves to the right as time increases and moves up as repairs occur probabilistically. As prescribed by the checkpoint strategy, the cell divides into two cells (yellow). The progeny may or may not be viable. B: In the timer strategy, once a checkpoint is activated, the cell arrests until time t' and then divides. The advancement boundary is a vertical line. C: In the repair threshold strategy, cells arrest until E' errors remain and then divide. The advancement boundary is a horizontal line. D, E: The optimal strategy could, in principle, be probabilistic (panel D) or deterministic (panel E).

Calculating the optimal checkpoint strategy

For comparison with the optimal strategy, we also analyzed two other plausible checkpoint strategies, a 'timer' override strategy (Fig. 2.2 B) and an 'error-threshold' override strategy (Fig. 2.2 C), described in the Supplementary Information.

In general, the optimal checkpoint strategy could be stochastic; that is, depending on the state of the cell and on predictions about future outcomes, the optimal decision could be to advance the cell cycle with a probability between zero and one. As explained in the Supplementary Information, we have proven that the optimal strategy is not stochastic (illustrated by a gray region in Fig. 2.2 D) but must be deterministic (dashed lines in Fig. 2.2 E). This means

17

that the optimal advancement probability $a(t,\{t_i\})$ is a Dirac delta (δ) function in t; the advancement probability can be represented by a sharp decision boundary in the error-time plane (Fig. 2.2 E), which we refer to as the 'advancement boundary'. Once a cell reaches this boundary, the optimal decision is to advance the cell cycle with probability one.
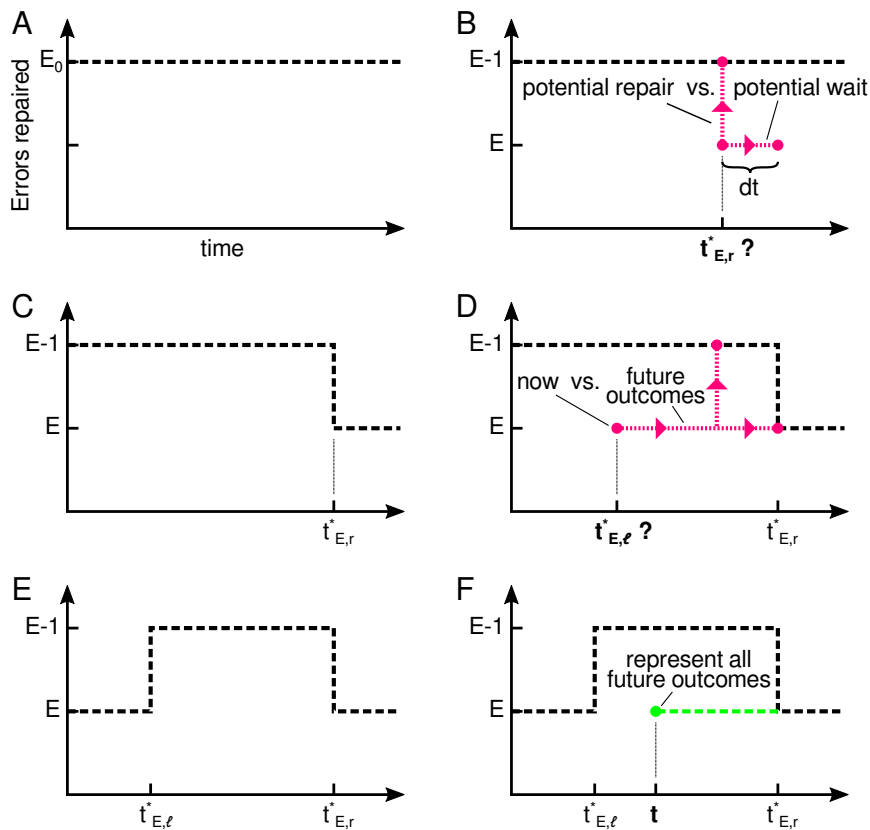
Fig. 2.3 – Steps for computing the optimal advancement boundary.

The problem of solving for the optimal strategy is, in principle, complicated because of the branching nature of the decisions; the consequences of a decision at time t and with $E(t)$ remaining errors depend on an infinite number of possible future events. However, the optimal checkpoint strategy can be solved recursively starting from the future and working backwards. Specifically, closed-form expressions for the advancement boundary can be found by analyzing the points in the error-time plane from right-to-left (future-to-present) and then from top-to-bottom (all-to-no errors corrected). In the following steps, we start with the trivial case where all errors have been fixed ($E = 0$, Step 1) and calculate the advancement boundary for E errors provided we have carried out the analysis for $E - 1$ errors already (Steps 2-5):

1. The survival probability is equal to one when all E_0 errors are repaired. It is obviously optimal to advance with the cell cycle when there are no errors ($E = 0$). Therefore, we draw an advancement boundary line at $E = 0$ (Fig. 2.3 A). Next, we iterate the following Steps 2-5:

2. For states with E unrepaired errors with an advancement boundary line at $E - 1$, we consider what happens when we increase t, keeping E fixed. At some time $t_{E,\mathrm{r}}^*$, it may cease to be worth waiting for another repair event. This time is reached when the conditional repair probability times the gain in fitness for making one more repair, $\frac{dt\partial_t\rho}{1-\rho}E\left(s(E-1)-s(E)\right)e^{-t/\tau}$, is outweighed by the loss of fitness if another repair does not occur ($-s(E)dt\partial_t e^{-t/\tau}$), depicted in Fig. 2.3 B. Equating these two terms and writing the survival probability in terms of independent contributions for each error, we obtain,

$$\boxed{\left.\frac{\partial_t\rho}{1-\rho}\right|_{t=t_{E,\mathrm{r}}^*} \approx \frac{\sigma}{E\tau}} \quad . \tag{2.2}$$

This simple relation allows the right advancement boundary $t_{E,\mathrm{r}}^*$ at E (Fig. 2.3 C) to be computed. (See Supplementary Information for additional details.)

Steps 3-5 of the computation and further details are presented in the Supplementary Information. In brief, in Step 3, after computing the right advancement boundary $t_{E,\mathrm{r}}^*$ in Step 2, we find whether the wait up to the right boundary is preceded by any times $t_{E,\ell}^*$ that should also trigger cell cycle advancement for the same number of E errors (Fig. 2.3 D, E). In Step 4, we find whether there are a series of such advancement-boundary—wait-segments before (to the left of) $t_{E,\ell}^*$, repeating Steps 2 and 3 for the same number of errors E from right to left (Fig. S3 A). Before moving down in the diagram and repeating this analysis for $E + 1$ errors in the recursive computation, the time points inside the gaps (wait times) between $t_{E,\ell}^*$ and $t_{E,\mathrm{r}}^*$ must be filled with predictions of the expected number of progeny if these time points are reached (green dashed line in Fig. 2.3 F). This is because the formulas in Steps 2-4 rely on the survival probability for cell cycle advancement with $E(t) - 1$ errors but if there is no advancement boundary at $E(t) - 1$, the expected number of progeny is the more general quantity to replace $s(E - 1)$ in those formulas. So, in Step 5, the gaps between advancement boundaries for E errors are filled with the expected number of progeny once a particular time

point in the gap is reached (Fig. S3 B).

The strategy encompasses two possible actions: i) wait for more potential repairs or ii) advance because waiting any longer brings down the expected offspring number. The reasons for advancement (ii) can be subtly different: Hitting a right border as in Fig. 2.2 E means that any further waiting is disadvantageous (waiting is hopeless); arriving at a left border, before it is optimal to wait, a number of repairs had to have been performed quickly, and any further improvements are unlikely to occur soon enough to be worth the wait (cash in a lucky draw); advancement at a top border can be interpreted either way.

The strategy is optimal by construction. Given that we start in the future and work backward, at each step we calculate the optimal decision based on having calculated the best decision for all accessible future time points.

2.3.2 Experimental results

Experimental system

To apply the theory, we created genetically mutated budding yeast strains. To avoid artificially creating templates for DNA repair by homologous recombination, we minimized the introduction of extraneous DNA, including markers, by using the *URA3*-insertion/5-FOA-pop-out method throughout.

We deleted the Start cyclins CLN1,3 and replaced the CLN2 promoter by the MET3 promoter. This allows cells to be blocked in the pre-Start (G1) phase prior to DNA replication by adding methionine to the growth medium (+Met) or to be released to start a new cell cycle by removing methionine (-Met).[94] Blocking cells in G1 prior to DNA replication, where haploid yeast cells only have one of each chromosome avoids efficient template-based repair mechanisms based on the homologous chromosome and allows the controlled generation of DSBs.

We further integrated a *GAL1pr-HO* construct in the genome. The enzyme Ho creates a DSB with a 4-nucleotide 3' overhang[31] at locations in the genome where we inserted, additionally, the short (30 bp) Ho recognition sequence. Ho has a natural cut site at the mating type locus (MAT), which we abolished in cells of mating type α by 10 synonymous mutations in the

alpha1 gene (MATα-syn). Ho is widely used to create DSBs to study checkpoints, override, and DNA repair.[31]
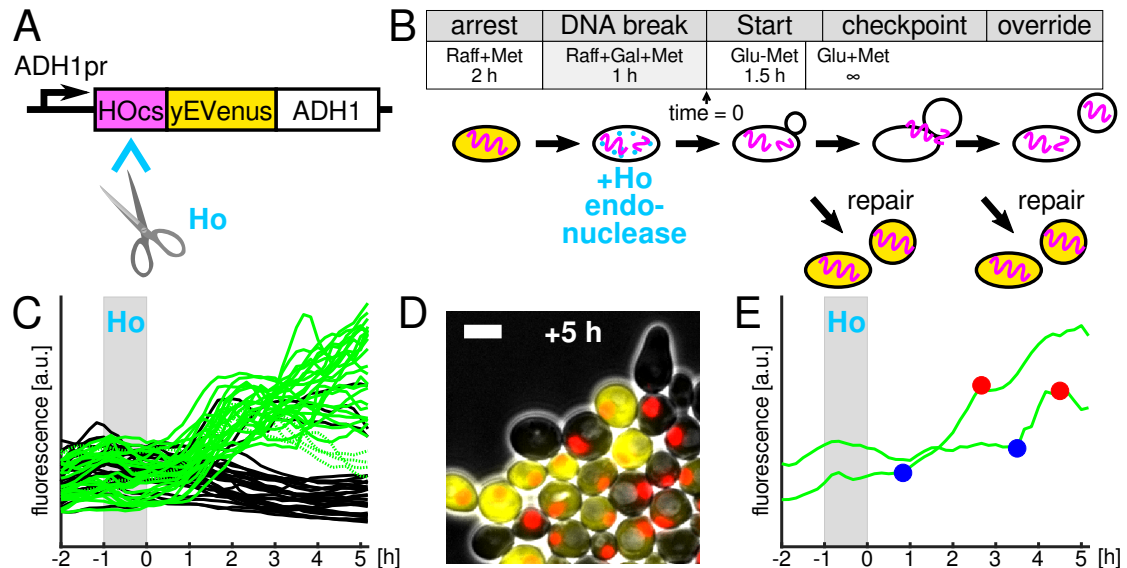
Fig. 2.4 – The *ADH1pr-HOcs-yEVenus-ADH1* DSB sensor reports the presence of a DSB. A: Design of the sensor. B: Basic experimental protocol illustrated with *cln∆ MET3pr-CLN2 GAL1pr-HO ADH1pr-HOcs-yEVenus-ADH1* strain. Raff = raffinose, Gal = galactose, Glu = glucose. C: YFP time courses in cells which additionally carry the *cdc5-ad* mutation. Green/black: cells that did/did not complete nuclear division. Four dead cells indicated by dotted lines. Switch to Glu-Met occurred at time 0 h. (n = 75) D: Cells 5 hrs after media switch to Glu-Met. Nuclear marker Htb2-mCherry in red. Scale bar: 5 μm. E: Examples of YFP time courses for cells that divided nuclei late but seemed to repair the DSB early. Time point of rise in fluorescence indicated by a blue circle; nuclear division indicated by a red circle.

To detect DSBs and their repairs in single cells under the microscope or by flow cytometry, we devised a simple trick: We inserted an HO cut site (HOcs) and a destabilized version of the yellow fluorescent protein gene yEVenus between the constitutive yeast promoter *ADH1pr* and the non-essential ADH1 gene, creating an *ADH1pr-HOcs-yEVenus-ADH1* fusion (Fig. 2.4 A) in place of the genomic *ADH1pr-ADH1* locus. (We refer to the yEVenus *protein* as YFP to simplify the figure labels and the text.) When the HO cut site suffers a DSB, yellow fluorescence should be low; when the DSB is repaired, yellow fluorescence should turn back on. Among other advantages, this system allowed us to induce Ho briefly in galactose medium, switch to the preferred carbon source glucose, and focus on cells with DSBs based on their fluorescence levels.

Thus, the basic genotype for all experiments described below is *cln1-3∆ MET3pr-CLN2 GAL1pr-HO ADH1pr-HOcs-yEVenus-ADH1 HTB2-mCherry* MATα-syn, and only modifications of this

strain are highlighted explicitly.

DSB repair distributions

A key input to the checkpoint theory is the repair probability distribution ($\rho(t)$ in Eq. (2.2)).
To quantify the timing of DSB repairs, we used the protocol depicted in Fig. 2.4 B: i) cells were
arrested in G1 phase to ensure that only one copy of each chromosome was present, ii) a
break was induced between *ADH1pr* and yEVenus by Ho, iii) the cell cycle was restarted, and
iv) a new cell cycle was prevented. Step (iv) allowed us to watch cells for many hours under
the microscope by preventing intact cells from dividing and overcrowding the field of view.
This was necessary to detect late, rare repair events. Furthermore, in order to use nuclear
division as an indicator of DSB repairs, we performed experiments with cells carrying the
well-characterized *cdc5-ad* mutation[2], which prevents checkpoint override, so that nuclear
division only occurred in the absence of DSBs.

To characterize the system, we performed single-cell fluorescence microscopy and analyzed
the images with the convolutional neural network YeaZ[95]. At the switch to Glu-Met, all cells
showed low fluorescence due to the induced DSB or low ADH1 expression in raffinose and
galactose. Subsequently, fluorescence shot up in all cells that divided their nuclei (Fig. 2.4 C).
Thus, only cells where the DSB was repaired (or had never been induced in the first place,
discussed below) divided. This underscores the effectiveness of override suppression by the
cdc5-ad mutation since we saw no YFP-negative (YFP-) cells that performed nuclear division.
Some cells did not divide their nuclei but showed a jump in fluorescence, indicating a failure
to complete the cell cycle even in the absence of a DSB. We investigated the four cells that
divided but showed low fluorescence after 5 hrs in Fig. 2.4 C (dashed lines) and found that
they did not grow noticeably, suggesting that they were dead. Thus, there was a clear gap
in fluorescence levels between cells that did not divide and had an unrepaired DSB and the
rest (Fig. 2.4 C, D). Furthermore, we compared the time when fluorescence increased and
when nuclear division occurred and found that in all cells with dividing nuclei, fluorescence
increased earlier than anaphase (examples of large differences between the two shown in
Fig. 2.4 E). Thus, the DSB sensor provided direct information about whether cells had a DSB
or not, which complements information provided by nuclear division. In the cells observed,

anaphase was always preceded by rising YFP levels but YFP could increase without anaphase, i.e., repair could occur but the cell cycle fail, nevertheless.
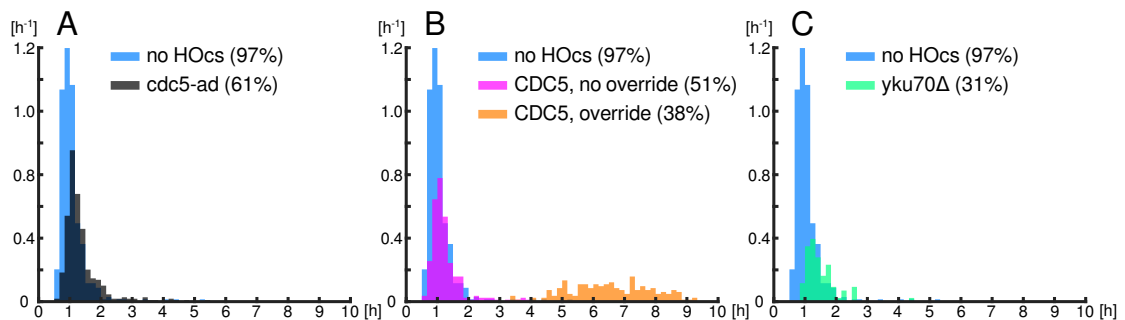
Fig. 2.5 – Rate of nuclear division with respect to budding scored by fluorescence microscopy. All divisions were accompanied by YFP increases except in panel B where dividing *CDC5* cells could fail to turn on YFP (checkpoint override). Percentage in parentheses indicates the fraction of the budding cells of each genotype that divided nuclei. These cells' budding-to-nuclear-division times are shown in the histograms. The same no-HOcs control cells are shown in all three panels for comparison. n = 656 (*cdc5-ad*), 493 (wt-*CDC5*), 413 (no HOcs), 259 (*yku70Δ*).

As a first estimate of repair times, we recorded the time from budding to nuclear division by fluorescence microscopy with 10 min time resolution. We verified that the *cdc5-ad* mutation neither affected repair timing nor repair efficiency negatively by comparing the division times of *cdc5-ad* cells with wild-type *CDC5* cells in which YFP turned on, i.e., did not override (61% vs. 51%, Fig. 2.5 A, B), in agreement with previous observations[29].

A substantial fraction of *cdc5-ad* cells (39% = 100% - 61%) did not divide compared to 3% of cell cycles failing under these conditions in a no-cut-site control strain (Fig. 2.5 A). Thus, approximately 36% (= 39% - 3%) failed to repair the DSB. The fraction of *cdc5-ad* cells that divided (61%) (Fig. 2.5 A) did not simply represent inefficient cutting by Ho. This is because only 31% of cells that additionally carried the *yku70Δ* (=hdf1Δ) deletion, which blocks the non-homologous end-joining repair pathway[6], divided, showing that 30% (= 61% - 31%) of cells repaired the DSB by a *YKU70*-dependent mechanism (Fig. 2.5 A, C). The fraction of dividing cells with the *yku70Δ* deletion is higher than in previous studies[22,89], possibly due to differences in the DSB loci, e.g., level of transcriptional activity around the cut site. As expected, in the *cdc5-ad* population (Fig. 2.5 A) there were cells that divided late, i.e., later than 2 hours after budding, 6.1%, which was significantly ($p = 2 \cdot 10^{-3}$, one-tailed) higher than when there was no cut site, 2.7%, representing late repair events. However, most *YKU70*-dependent repairs (NHEJ) clearly took place very quickly (Fig. 2.5 A, C).
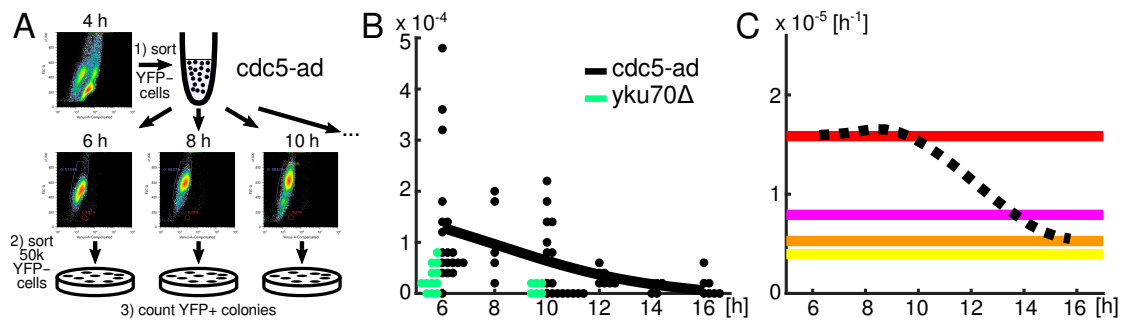
Fig. 2.6 – Measurements of late DSB repair statistics and survival rates after checkpoint override. A: Schematic of FACS experiments to measure the tail of the DSB repair time distribution. Horizontal and vertical axes on FACS plots are Venus-A and FSC-A, respectively. See Fig. S4 for more details. B: Measurements of the fraction of repaired cells (YFP+ colonies) compared to the number of cells plated ($5 \cdot 10^4$). Each circle represents the fraction of YFP+ colonies among 50k cells on one plate. Circles are stacked horizontally when experimental replicas had the same numbers of colonies. The thick black line represents a spline fit to the mean values for *cdc5-ad* cells at each time point. C: The probability distribution function of repair (dashed line), which is the negative of the derivative of the fit in panel B. Horizontal lines represent $\sigma/(E\tau)$ for $E = 1$ (red), 2 (magenta), 3 (orange), 4 (yellow).

The long tails of the distributions observed by microscopy (Fig. 2.5) are potentially critical to understanding checkpoint override. However, statistics on the rare events that make up the tail were by their nature difficult to ascertain accurately by single-cell microscopy. Thus, we took advantage of the strong fluorescence signal of the *ADH1pr-HOcs-yEVenus-ADH1* reporter to analyze cells by fluorescence-activated cell sorting (FACS) (Figs. 2.6 A, S4). At +4 hrs after the switch to Glu-Met (Fig. 2.4 B), $>10^6$ YFP- cells were isolated. To avoid contamination by YFP+ cells, we chose the gates for the FACS conservatively, based on the width of the distribution of fluorescence in a no-cut-site control strain (Fig. S4 C). (The *yku70Δ* results, discussed below, indicate that stray low-fluorescence but uncut cells, which would contaminate the results, were dead or negligible.) Then, from this population, multiple batches of 50 000 YFP- cells were sorted and plated on Glu-Met plates every 2 hours. On Glu-Met plates, cells could generate colonies if they repaired the DSB eventually since the absence of methionine reactivated the MET3pr-CLN2 construct and allowed new cell divisions. The double sorting, once at 4 hrs and once before plating, served to minimize the possibility that sorting errors let bright (YFP+) cells slip through as YFP- cells. After 3 days, we counted the number of all colonies on the plates and determined the subset of YFP+ colonies. With *yku70Δ* cells, substantially fewer colonies emerged, showing that nearly all colonies represented *YKU70*-dependent repairs by non-homologous end joining (Fig. 2.6 B, Fig. S4 B), and not technical artefacts. The number of YFP+ colonies decreased rapidly between the 6 h to 12 h time points (Fig. 2.6 B), showing that

some YFP- cells had repaired the DSB between sorting events, had turned YFP back on, and had left the population of YFP- cells between time points. We estimate that for a typical YFP- cell, it took approximately 30 min to leave the YFP- population, as delimited by our FACS gate, once it repaired the DSB (see Methods). The total number of colonies, that is, YFP+ and YFP- combined, did not drop appreciably between the 6 h to 16 h time points (Fig. S4 D); this shows that the precipitous drop in YFP+ cells with time was not because cells were generally dying during the long arrests. Because the number of YFP- colonies did not change substantially within a very long time span (6 h-16 h), these colonies likely arose from cells that repaired the DSB early but which destroyed the DSB sensor in the process and became permanently YFP- cells.

To extract the repair probability in an unbiased manner, we fit a spline through the mean fractions of repaired cells (Fig. 2.6 B). The negative of the derivative of the fit represents the conditional probability density function for DSB repair, $\partial_t \rho/(1-\rho)$, indicated by a dashed line in Fig. 2.6 C.

Statistics of survival after checkpoint override

Another crucial quantity determining the balance between risk and speed is the lethality of overriding the checkpoint with unrepaired damage (Eq. (2.2)). We measured the survival probability $s(E)$ for one DSB ($s(1) = \sigma$) by repeating the experiment in Fig. 2.4 with wt-*CDC5* cells. We plated *CDC5* cells at the 6 h time point, just as cells were beginning to override the DNA damage checkpoint and after most pre-override repairs had taken place (Figs. 2.5 B, S4 E). Subtracting the survival probability of *cdc5-ad* cells, similarly sorted at +6 h to further remove the contribution of pre-override repairs, we arrived at the mean survival probability σ, which is represented, after dividing by the cell cycle time $\tau = 90$ min/log 2, by the red horizontal line in Fig. 2.6 C.

Quantitative experimental validation of theoretical predictions

We begin with a comparison of theory and experiment for one DSB ($E = 1$). The red ($\sigma/(E\tau)$) and dashed lines ($\partial_t \rho/(1-\rho)$) overlap very well in the time window 6-9.5 h (90% or 95%

bootstrap confidence intervals: $\partial_t \rho / (1 - \rho)$ is within 25% or 33% of σ / τ, respectively, in the 6-10 h window, see Methods). Remarkably, the measured override time in Fig. 2.5 B is 7.4 ± 1.4 h (mean $\pm$ STD) or 7.3 ± 1.3 h (median, 20th to 80th percentile) (n = 188). (Note that the microscopy results, e.g., in Fig. 2.5 B, show bud-to-nuclear-division times, to which the time from +0 until budding has to be added for each cell (≈ 50 min) to compare to FACS results.) Our measured override times for 1 DSB agree with the override time of ≈ 8 h reported in multiple past studies.[1,2,27] Thus, the optimal checkpoint theory explains for the first time the mean as well as the broad width of the override distribution for 1 DSB.

We wished to make new, untested predictions. Assuming that each DSB reduces the survival probability independently, $s(E) = \sigma^E$, we predicted the optimal override time for multiple DSBs using Eq. (2.2). The repair probability distribution $\partial_t \rho / (1 - \rho)$ intersects $\sigma / (E\tau)$ at approximately 13.8 h for $E = 2$ DSBs and 16.2 h for $E = 3$ DSBs. A linear extrapolation of the last half hour of $\partial_t \rho / (1 - \rho)$ intersects $\sigma / (E\tau)$ at 19.1 h for $E = 4$ DSBs. These predictions contrast with previous override measurements for 2 DSBs by DNA content quantification in bulk culture[27], which did not detect override for the duration of the experiment (24 hrs). This led to the conclusion that cells do not override in the presence of 2 DSBs.

To compare to our theoretical predictions and to revisit these past experimental results, we inserted additional DSB cut sites at the *URA3* locus or in the promoters of *DLD2* or *MIC60*. *URA3* was chosen for comparison with previous work[27]. *DLD2* and *MIC60* are in long (≈ 10 kB) regions of the yeast genome which can be deleted without affecting viability.[96] Measurements were performed as before by single-cell timelapse microscopy where budding and anaphase were scored. Because in these strains, not all cut sites had a fluorescent reporter, we had to modify the protocol in Fig. 2.4 B; this made the procedure similar to previous studies[1,2,27]: We kept *GAL1pr-HO* on by switching to Gal-Met medium instead of Glu-Met after time 0, to ensure that cut sites would be recut and could not be repaired.[89] Thus, nuclear divisions now only occurred after checkpoint override; DSB repair resulting in a restored cut site and subsequent normal nuclear division were suppressed. The alternative possibility that error-prone repair allowed normal divisions, because Ho could no longer recut the corrupted Ho recognition site, was too rare (probability $\approx 10^{-3}$)[97] to have affected our measurements. We assessed how much galactose medium in this modified protocol affected override times and found a

relatively small change to 8.9 ± 0.3 h (mean $\pm$ SEM, n = 53, bud to nuclear division) with the single DSB in *ADH1pr-HOcs-yEVenus-ADH1*.
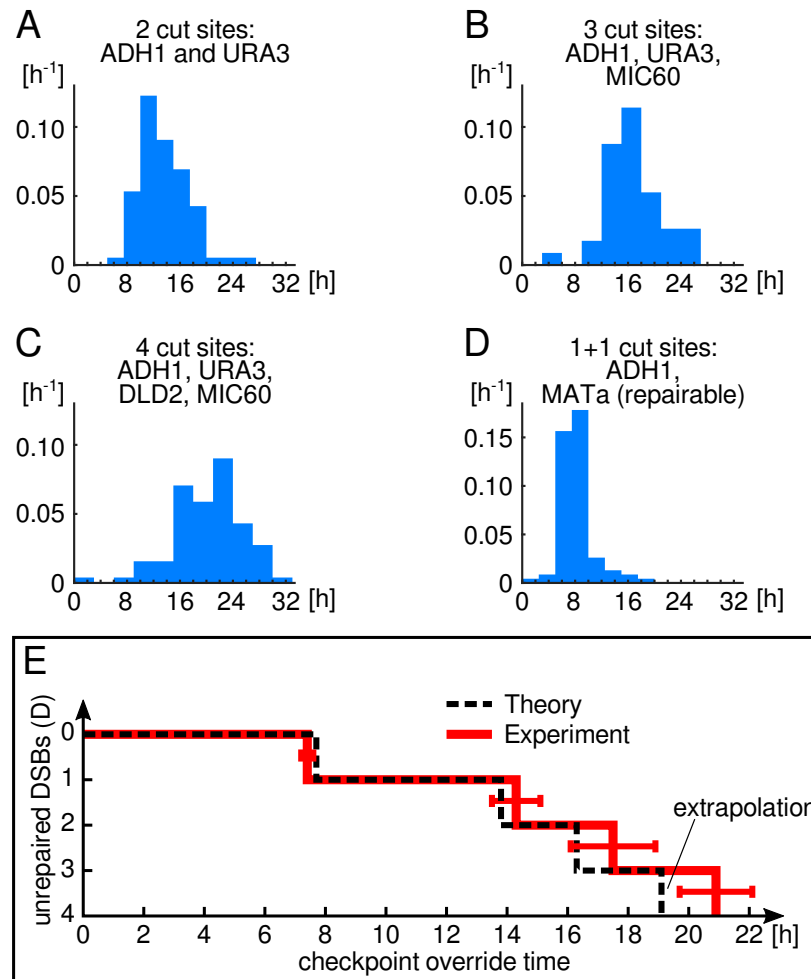
Fig. 2.7 – The optimal checkpoint theory predicts DNA damage checkpoint override times. A-D: Histograms of budding-to-nuclear-division probabilities for cells with multiple cut sites (n = 75, 38, 85, 92). E: Comparison of the optimal checkpoint theory with the experimental data. 50 min have been added to the means from the bud-to-nuclear-division histograms because the FACS time points are with respect to time 0 in the experimental protocol. Horizontal red error bars indicate 95% confidence intervals.

Strikingly, our results differ from previous conclusions based on bulk culture measurements[27] but agree with the predictions of the optimal checkpoint theory (Fig. 2.7 E): For two cut sites at ADH1 and *URA3* we observed that 80% of cells overrode with bud-to-nuclear-division time 13.4 ± 0.4 h (mean $\pm$ SEM, n = 75) (Fig. 2.7 A). For the two cut sites at *DLD2* and *MIC60*, the mean override time was very similar, 13.6 ± 0.4 h (mean $\pm$ SEM, n = 88, bud-to-nuclear division) (Fig. S5 A). For three and four cut sites, the fraction of overriding cells decreased (34% and 42%) while the proportion of clearly dead cells, e.g., cell wall ruptured, increased.

Nevertheless, for cells which performed nuclear divisions, we measured the override times to be 16.6 ± 0.7 h (mean $\pm$ SEM, n = 38, bud-to-nuclear division) for 3 cut sites and 20.2 ± 0.6 h (mean $\pm$ SEM, n = 85, bud-to-nuclear division) for 4 cut sites (Fig. 2.7 B, C). Note that these shifts in override timing as a function of DSB numbers cannot be explained by the greater lethality of increasing numbers of DSBs since the above override times are computed based only on the observed checkpoint overrides, not by averaging with non-overriding or dead cells. Thus, the match between theory and experiment is remarkably close (Fig. 2.7 E), especially considering the disparate nature of the experiments and the substantial cell-to-cell variability.

Thus far, we have compared our theoretical results for $E = 1$ DSB to experiments in which we ensured that cells had the DSB at the time of override by using the *ADH1pr-HOcs-yEVenus-ADH1* sensor and focusing on YFP- cells. For $E = 2$, 3, or 4 cut sites, we ensured that DSBs were maintained throughout the experiment by continuous HO induction. (We repeated the $E = 1$ DSB experiment with continuous HO induction as well.)

Finally, we also wished to examine the predicted advancement boundary in a more complex way. We wondered whether the override decision could be confused by a decoy. To quantify more complex explorations of override decisions, we created a strain in which one DSB would be repaired efficiently and another DSB not. To accomplish that, we replaced MATα-syn at the mating type locus, which could not be cut, by the wild-type MATa site, which could be cut, in our DSB sensor (*ADH1pr-HOcs-yEVenus-ADH1*) strain. When MATa is cut by Ho, the DSB is repaired efficiently by homologous recombination based on the HML and HMR cassettes in the same chromosome.[98] The *ADH1pr-HOcs-yEVenus-ADH1* site, of course, still harbored the cut site without homology elsewhere in the genome, for which thus template-based repair was not available. We returned to our original experimental protocol in which Ho is shut back off (Fig. 2.4 B). (We extended the induction window of *GAL1pr-HO* while cells were arrested in G1 to 3 hrs to ensure that in a large fraction of cells both MATa and *ADH1pr-HOcs-yEVenus-ADH1* would be cut initially.) Control cells with only the cut site at the MATa locus divided their nuclei very quickly after switching to Glu-Met (median: 75 min), showing that, indeed, MATa was repaired efficiently. However, in combination with the *ADH1pr-HOcs-yEVenus-ADH1* sensor, YFP- cells overrode after 8.1 ± 0.2 h (mean $\pm$ SEM, n = 92, bud-to-nuclear division, Fig. 2.7 D), as expected for 1 DSB and unlike for 2 DSBs (Fig. 2.7 A). These results support our

theoretical analysis, in which cells compute the optimal override decision continuously as they move in the error-time plane, and adjust their override time based on $E(t)$, the present number of DSBs, as illustrated in Fig. 2.2 E.

Override is an advantageous strategy

The close match between predicted and measured override times (Fig. 2.7 E) suggests that checkpoint override may indeed be an advantageous strategy. However, this has not been shown directly in the past except with crippled DNA repair and maintenance genes[28,32,33], leaving the question open, to what extent checkpoint override is relevant to wild-type cells. In preliminary tests, we found a simple comparison of overriding (*CDC5*) to non-overriding (*cdc5-ad*) cells with one HO cut site under continuous HO induction inconclusive (data not shown). We speculated that most repairs occur well before checkpoint override (<6 hrs) and thus swamp the effects of checkpoint override (>6 hrs) on survival. Therefore, we compared *CDC5* and *cdc5-ad* YFP- cells at the 6 h time point directly, using the protocol described in Fig. 2.6 A. We found a significantly higher probability of survival for *CDC5* cells versus *cdc5-ad* cells (Fig. S5 B), showing that override is beneficial for cells with wild-type repair genes when they continue to have an unrepaired DSB late into the checkpoint arrest.

2.4   Discussion

We have shown that DNA damage checkpoint override follows predictable patterns. We presented the first theory of checkpoint strategies, which led us to discover these timing hierarchies.

Fundamentally, the theory is based on the simple principle of offspring maximization; a population genetics analysis showed that the probability of producing live progeny multiplied by an exponential time penalty for arrest should have been the target to be maximized in the course of evolution. In reality, this maximization would have been performed by selection: Given two genetically encoded strategies, one closer to the optimum and one less optimal, the more optimal strategy would have produced more progeny and won out over evolutionary timescales – until a strategy even closer to the optimum would have displaced it in the population.

The theory is general in that it is compatible with both canonical models of population genetics, exponential growth as well as fixed-size populations. We demonstrated the latter by analyzing both the classical Wright-Fisher and Moran models. Furthermore, the theory is also general because it describes fundamental balances between risk, represented by repair and survival probabilities, and growth. It would presumably apply to other biological surveillance systems, including the examples discussed below, even though in our presentation of the theory we anticipated the application to the DNA damage checkpoint. It can be extended straightforwardly, for example, to allow for sick cells.

We proved that according to the theory, a deterministic strategy is optimal. This may appear to be difficult to reconcile with the observed broad distribution of checkpoint override times (Fig. 2.5 B). However, the DSB repair probability is roughly flat for 6 h-10 h and then decays slowly (Fig. 2.6 C); thus, broad distributions of override times are compatible with a deterministic strategy since the optimal range is wide.

To solve for the optimal strategy, we mapped the problem of maximizing the fitness functional (Eq. (2.1)) onto the question of finding the optimal boundary for a random walk and derived closed-form recursive solutions. These can be calculated easily, e.g., the simple relation in Eq. (2.2). Simulations are not needed.

The theory establishes relationships between three independent quantities, i) the probability distribution of error correction, ii) the survival probability if errors are not fixed, and iii) the optimal timing of checkpoint override. The theory makes quantitative predictions for the override time as a function of the number of errors.

Experimentally, we built a budding yeast system which could be arrested in G1, a controlled number of DSBs could be induced, and the cells with DSBs could be separated from intact cells based on the fluorescence output of the DSB sensor. This allowed us to switch to glucose as the carbon source, which switched HO expression back off and permitted cells to repair the DSB. The fluorescent DSB sensor also allowed us to eliminate repaired cells by flow cytometry, which pollute experiments with checkpoint-arrested cells because intact cells divide and overwhelm bulk measurements exponentially quickly. The alternative, keeping cells in galactose, was not an option because Ho would continuously recut the DNA (until the DSB would be repaired

non-conservatively in a small fraction of cells). We used continuous HO induction in galactose only to measure override times.

This experimental system allowed us to measure the parameters (i) and (ii) and the predictions (iii) precisely. The theory predicted the override times as a function of the number of DSBs strikingly well. The discrepancies between theory and experiment are less than 7% for ≤ 3 DSBs. The predictions and experimental data are non-trivial. The override times vary by finite amounts as a function of the number of DSBs. These finite shifts were predicted well by the theory.

It is also interesting that the theory compelled us to reexamine the current view[29,31,33] that override only occurs for 1 DSB and not 2 Ho-induced DSBs[27], which implied that checkpoint override is limited and not a universal response to DNA damage in wild-type cells. Instead, we found override to occur with up to 4 DSBs. We verified our override time measurements with two different DSB pairs, at ADH1 and *URA3* or at *MIC60* and *DLD2* (Figs. 2.7 A, S5 A). We speculate that the wide distribution of override times for ≥2 DSBs (compare the variability for 2 DSBs in Figs. 2.7 A, S5 A to the variability for 1 DSB in Fig. 2.5 B), DNA re-replication after override, and slow post-override cell cycles hid the small fraction of post-override (1C DNA content) cells in bulk culture DNA content measurements at the time points 6 h, 12 h, 18 h, and 24 h in previous experiments[27]. This explanation is supported by our single-cell microscopy results with the 2 DSB strain YSL53 from previous work[27]: To have the same level of control over cell cycle entry and the same readout as in the rest of our experiments, we introgressed *cln*Δ *MET3pr-CLN2* HTB2-mCherry from our strains partially into YSL53 by a cross and three backcrosses with YSL53. We picked four different strains after the third backcross and found in all four that checkpoint override did occur with two cut sites.

Our detection of override with at least up to four DSBs also brings the basic observations about DNA damage checkpoint override more in line with each other. Override has been documented with difficult-to-quantify but plausibly large amounts of DNA damage due X-rays[28] or telomere dysfunction in *cdc13-1*[2] or *tlc1*Δ[29] cells. Our results revise the current view[33] that different types of DSBs must have different effects on override; varying numbers of DSBs led to quantitatively but not qualitatively different override times in our measurements.

Furthermore, the previously reported override block with 2 DSBs supported a molecular model in which the amount of post-break DNA resection, potentially signaled by the amount of ssDNA-bound RPA, determines whether or not override occurs.[27] The threshold on resected ssDNA allowing override would be between the amount produced in response to 1 to 2 DSBs. However, the discovery of mutants that produce less post-break DNA resection but also did not override have represented a challenge to this model.[31] Our results are in principle consistent with a modified, graded molecular model in which increasing amounts of ssDNA due to additional breaks increase the arrest duration by finite amounts.

Finally, we measured the biological relevance of checkpoint override on cells without crippling DNA repair or maintenance. We filtered for cells that had not repaired their DSB shortly before override occurred and saw a significantly greater chance of survival for override-performing (*CDC5*) cells.

The quantitative, system-level study we present here complements the more developed but nevertheless incomplete understanding of checkpoint override at the genetic level.[6,31] As in other fields, these two perspectives can be expected to drive each other forward. For example, the computations we uncovered here must presumably be performed at the molecular level by a complex machinery involving *CDC5*[2], *RAD53*[34], *PTC2* and *PTC3*[30], and other genes[6,31]. Quantitative measurements of the kinetics of these elements, e.g., as for DNA resection rates[27], combined with molecular modeling ought to be able explain the system-level computations we predicted from the bottom-up.

Theory ideally compels new kinds of experiments to uncover previously hidden patterns. A powerful aspect of a general, first-principles theory is that it can apply to disparate systems; the generality of the mathematical abstractions means that the specifics of the override are not important, for example, whether the checkpoint signal is silenced before override. (This is why we avoided the more specific term 'adaptation', which is more common in the literature.) To facilitate such further experimental exploration, we discuss in the Supplementary Information, on the basis of the existing literature, how the theory can potentially be applied to explain or predict override timescales of other checkpoints, including the spindle assembly checkpoint, in development, and in cancer cells.

2.5 Methods

2.5.1 Strains

We performed experiments in budding yeast strains of background W303. Genetic manipulations and crosses were performed by standard methods. The *cdc5-ad* mutation was cloned into our strain background from a strain given to us by Achille Pellicioli. A *GAL1pr-HO* plasmid was given to us by Eric Alani.

All ORF deletions and HOcs insertions were performed using the *URA3*-insertion/5-FOA-pop-out method. This method leaves no markers and no unwanted DNA in the genome. For this, the desired sequence of DNA was cloned into a *URA3*-backbone plasmid. After integration at the desired locus, cells were plated on 5-FOA plates. Colonies that grew on these plates were screened for the desired ORF deletion or HOcs insertion.

The basic genotype for all strains was *cln1Δ0 cln2Δ0::MET3pr-CLN2* (promoter replacement) *cln3Δ0::GAL1pr-HO ADH1pr-HOcs-yEVenus-ADH1 HTB2-mCherry::HIS5* MATα-syn. The modifications to this strain are indicated in Table 2.1. After constructing the basic strain, we performed three backcrosses with our wild-type W303 strains to reduce the likelihood of mutations.

Table 2.1 – Strains used

AS18	-	rad5-G535R
ET47	-	*RAD5*
AS20.1	*cdc5-ad*	rad5-G535R
ET45	*cdc5-ad*	*RAD5*
AS30	*yku70Δ0*	rad5-G535R
ET46	*yku70Δ0*	*RAD5*
ET44	*ADH1pr-yEVenus-ADH1* (no *ADH1pr-HOcs-yEVenus-ADH1*)	*RAD5*
AS31.9	*ura3Δ0::HOcs::KanMX*	rad5-G535R
AS32.1	*ura3Δ0::HOcs::KanMX*	*RAD5*
ET32	*MIC60pr::HOcs DLD2pr::HOcs* (no *ADH1pr-HOcs-yEVenus-ADH1*)	rad5-G535R
RD58	*MIC60pr::HOcs DLD2pr::HOcs* (no *ADH1pr-HOcs-yEVenus-ADH1*)	*RAD5*
RD53	*ura3Δ0::HOcs::KanMX MIC60pr::HOcs*	*RAD5*
RD54	*ura3Δ0::HOcs::KanMX MIC60pr::HOcs DLD2pr::HOcs*	*RAD5*
AS14.2	MATa (no *ADH1pr-HOcs-yEVenus-ADH1*)	*RAD5*
AS35.2	MATa	*RAD5*

HOcs stands for the 30 bp sequence: TTCAGCTTTCCGCAACAGTATAATTTTATA.

We performed experiments with cells carrying the W303-specific rad5-G535R mutation[99] as well as with cells with a corrected *RAD5* gene wherever we indicate both versions of the strain in the list above. Since we observed no systematic or noticeable differences between results with rad5-G535R and *RAD5*, we pooled the measurements for higher statistical certainty. All other experiments were performed with cells with a corrected *RAD5* gene only.

2.5.2 Media changes and sonication

The standard protocol for all experiments, except where the protocol was modified as noted, is depicted in Fig. 2.4 B. Cells were pre-grown in 5 ml Raff-Met liquid medium for 24-48 hours, then diluted at 18:00 in the evening before the experiment to OD=0.005. The first step of the protocol, the switch to Raff+Met, was performed at around 9:00 on the next morning. For bulk culture experiments, the OD was maintained below 0.5.

Cells were sonicated for 10 sec at 40% power on a Sonics & Materials VCX 500 instrument for single-cell experiments immediately before loading into the microfluidic chip. For bulk culture experiments, the culture tube containing cells was placed in a Branson bath sonicator for 8 sec before FACS sorting (see below).

2.5.3 Microscopy

Microscopy experiments were performed with commercial microfluidic chips. Timelapse recordings were carried out with a 60x objective and a Hamamatsu Orca-Flash4.0 camera. Widefield images were taken in phase-contrast mode. Fluorescence images were taken with a Lumencor Sola SE II light source. The filter cubes were a Semrock YFP-2427B (excitation: 500/24, emission: 542/27) and a Semrock mCherry-C (excitation: 562/40, emission: 641/75). All exposure times were 100 ms at 50% light source power. The interval between images was 10 min except for experiments with ≥2 cut site where the time between images was increased to 15 min to decrease potential phototoxicity during the long arrests. The override time was recorded as the first time point at which the Htb2-marked nuclei separated. In microscopy experiments where we released cells from Gal+Met into Gal-Met (Fig. 2.7 A-C), there were

sometimes 1-2 cells that divided immediately and then arrested in the next cycle. We excluded these if this first division occurred within the first 100 min.

2.5.4 Image processing

For segmenting the microscopy images, we used the YeaZ convolutional neural network and GUI[95].

2.5.5 FACS

Fluorescence-activated cell sorting was performed with a Sony SH800S instrument. The protocol and all the gates are illustrated in Figs. 2.6 and S4.

The instrument was set to room temperature for sorting events. A 100 μm microfluidic sorting chip was used. The purity level was set to 'ultra purity'. We used the excitation/emission filters for 'Venus'.

Before each sort, cells were centrifuges at 900 g for 1.5 min, medium was removed to concentrate cells, and the cell culture was sonicated for 8 sec. This was done to speed up the sorting. At the 4 h time point, $1.0 - 1.8 \cdot 10^6$ YFP- cells were isolated per biological replica, which took about $20 - 40$ min. After sorting, cells were centrifuged, the sheath medium was discarded, and ≈ 5 ml SCD+Met medium was added. Cells were always kept on a nutator at 30° C between sorting events. The second sorting events of 50k YFP- cells at 6 h, 8 h, 10 h, 12 h, 14 h, or 16 h took $3 - 8$ min. After the second sorting, 100 μl of SCD-Met medium was immediately added to the isolated cells and each batch of 50k YFP- cells was spread on a different Petri dish with SCD-Met agar medium.

To estimate the time it took cells to escape the YFP- gate after repairing the cut site at *ADH1pr-HOcs-yEVenus-ADH1*, we noted that at the 4 h sorting event, YFP- and YFP+ cells showed fluorescence levels of 1700 ± 700 [au] (median $\pm$ SD) and 7500 [au] (median), respectively. The speed of increase of fluorescence per hour therefore was about 1500 [au]/h, which is more than twice the standard deviation of fluorescence values in the YFP- gate. Hence, we estimate the escape time for repaired cells from the YFP- gate to be about 30 min.

2.5.6   Fit to data

In Fig. 2.6 B, we fit a 'SmoothingSpline' through the means at each time point using the Matlab 'fit' function with parameter 'SmoothingParam' set to 0.1. A spline was used to avoid any biases regarding the functional form, e.g., type of decay, we might have expected. The smoothing parameter was chosen without fine-tuning; thus, it only has one significant digit. It was chosen among such one-significant digit values because it was the highest such number (generating the least amount of smoothing) that removed the bumps from the fit.

2.5.7   Statistical tests

All p value tests were one-tailed. For the confidence interval analysis of the repair probability versus σ/τ in Fig. 2.6 C, we picked 10^3 random alternative means for each time point (6 h, 8 h, 10 h, 12 h, 14 h, and 16 h) by bootstrapping. We fit the same spline as described above through 10^3 combinations of these means and computed the derivative. We calculated how close the closest 90% and 95% of these conditional repair probability densities were to the σ/τ line between the 6 h and 10 h interval, which gave us the values quoted in the text (25% and 33%, respectively).

2.6 Supplementary Information

2.6.1 Supplementary theoretical results

Outcome options: survival or death

Focusing only on the possibilities that cells either die or survive was supported by our observations in all DNA break experiments that the surviving cells grew into colonies of roughly the same size at about the same speed. Thus, we did not observe two different colony sizes, which would suggest healthy and sick survivors.

Similarly, other researchers have scored viability by counting the number of colonies that have been formed from single surviving cells without noting sick colonies.[54,89]

Galgoczy and Toczyski[28] observed colonies growing at different speeds after exposing diploid cells that could not repair DSBs by homologous recombination (*rad52Δ*) to X-rays. Diploid cells can survive the loss of a chromosome and become aneuploid. Thus, sickness may have been a more common outcome under those conditions than for haploid cells.

Furthermore, in reality, sick cells would be outcompeted exponentially quickly in time and thus would be effectively dead except in special circumstances, e.g., spatial isolation or immediate post-arrest mating and random assortment of the chromosomes generating a subset of healthy offspring. These more complicated scenarios may be considered for further developments of the theory but we did not find those to be necessary because of the excellent match between theory and experiment.

In any case, the theory can be easily extended by introducing additional parameters describing the statistics of the occurrence and degree of sick cells.

Additional information on the arrest penalty

In a fixed-size population of N cells reproducing according to the Wright-Fisher model[91], the survival probability of an arrested cell is $\left(1 - (1 - 1/N)^N\right)$ per generation. This factor represents the probability that the arrested cell is not lost from the population due to drift,

which would occur if the $N - 1$ other cells in the population were selected to reproduce N times by chance. The probability of survival decreases from $3/4$ for $N = 2$ to $1 - e^{-1} = 0.63...$ as the population becomes larger ($N \to \infty$). Since in this model, the checkpoint-arrested cell either dies or survives and then rejoins the regular population dynamics as before the arrest, the expected number of progeny is reduced by $P_1 \left[1 - (1 - 1/N)^N\right]^{t/T}$ for a checkpoint arrest of t/T generations.

In a Moran process, the survival probability due to random drift is $(1 - 1/N)$ for a checkpoint-arrested cell, which is the probability that the cell is not killed with probability $1/N$. However, in a Moran process, it takes N generations on average for each cell to have its turn in reproduction because only one cell's fate is considered in each generation. Thus, adjusted for the smaller time steps in this model compared to the Wright-Fisher model, the survival probability in the presence of drift is $(1 - 1/N)^N$ per N generations in this model, which increases from $1/4$ for $N = 2$ to $e^{-1} = 0.37...$ for $N \to \infty$. The expected number of progeny after checkpoint arrest is thus $P_1 (1 - 1/N)^{Nt/T}$.

Thus, in all models, the expected number of progeny of a checkpoint-arrested cell is reduced by the product of a temporal penalty for arrest, which is exponential in time, and a probability of proliferation. In exponential growth, the fitness penalty due to checkpoint arrest ($2^{-t/T}$) is exponential in time with base $1/2$. In the Wright-Fisher model, the base of the exponential penalty depends on the size of the population; in each generation, the probability of survival decreases by a factor of $1 - (1 - 1/N)^N$. In a Moran process, the equivalent factor is $(1 - 1/N)^N$. Interestingly, while these processes are very different, the loss of expected progeny per generation due to waiting is roughly similar numerically.

We represent the time penalty by a factor $e^{-t/\tau}$, which applies in all three cases and where τ absorbs the logarithm of the base, that is, $\tau = T/\log 2$ for exponential growth, $\tau = -T/\log\left(1 - (1 - 1/N)^N\right)$ for the Wright-Fisher model, and $\tau = -T/\log\left((1 - 1/N)^N\right)$ for the Moran model.

Fitness: arithmetic vs. geometric mean

To illustrate that with random checkpoint arrests, the average of the offspring numbers is an appropriate fitness function, we consider the following simple exponential growth model:

1. Starting with one cell, every cell produces two offspring with probability $(1-q)$ in every generation.

2. With probability q, a cell suffers damage, which is either lethal with probability $(1-p)$ or which is repaired with probability p and delays reproduction by g generations.

The expected number of offspring $\langle \text{offspring} \rangle$ for this model after G generations is approximately:

$$\langle \text{offspring} \rangle = \left(2(1-q) + 2^{-g} pq \right)^{G} \quad , \tag{S1}$$

where $2(1-q)$ is the expected number of new cells due to normal divisions (model step 1) and $2^{-g} pq$ is the expected number of cells which resolve the damage after arresting at the checkpoint for g generations (model step 2).

As the simulations of the model in Fig. S1 show, the above equation for the average number of offspring ($\langle \text{offspring} \rangle$) captures the main peak of the distribution well. Thus, the average is a useful indicator for the behavior of the population. Given that the incidence of damage q is random and set by processes other than checkpoint control, we can only increase the average number of offspring by maximizing the product $2^{-g} p$, as we did to find the optimal checkpoint strategy.

If, by contrast, we consider a fluctuating environment model in which a whole generation – not random cells – suffers damage with probability q which is lethal with probability $(1-p)$, then in each generation, the chance of survival goes down by a factor of $(1-q(1-p))$. The survival probability thus goes to zero with time, and the average number of offspring after many generations would be dominated by unlikely scenarios where cells survive for long times and with many offspring. In these types of models the more appropriate fitness function to maximize would be the expected number of offspring for a typical (average) scenario, which leads to bet hedging.[93]

Additional information regarding the general fitness functional

To make the mathematical presentation simpler, we assume in Eq. (2.1) and in the subsequent calculations that if cells survive after cell cycle division, it is either always one of the
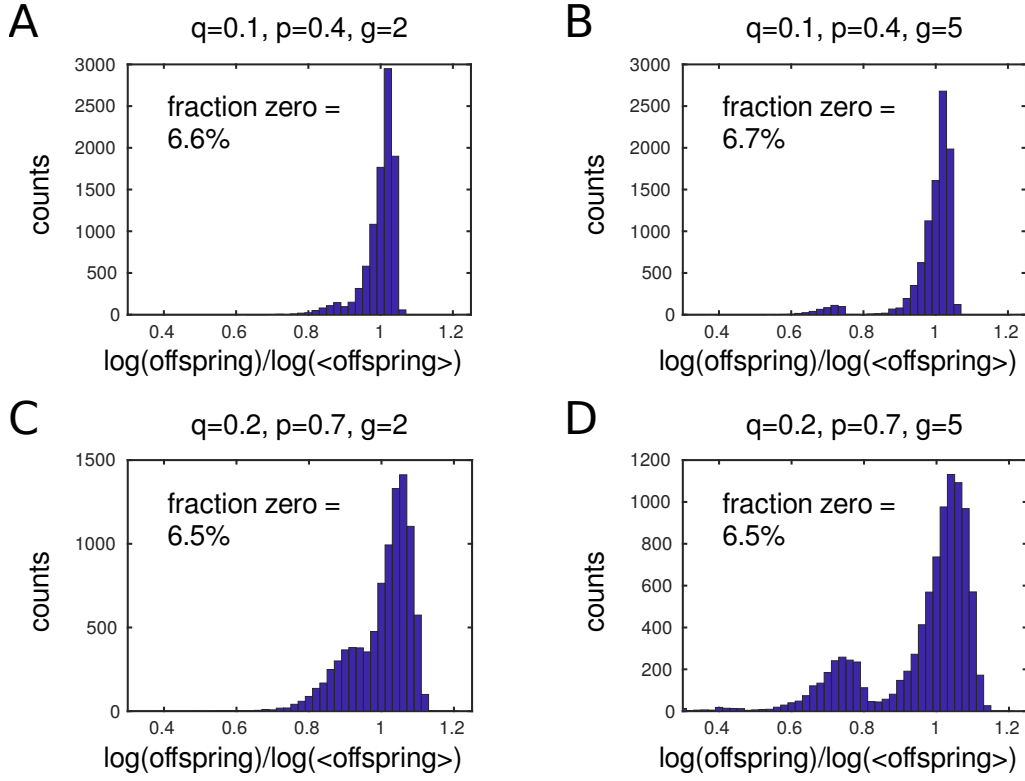
Fig. S1 – Distribution of offspring numbers for a simple population model of damage and checkpoint arrest, as explained in the Supplementary Information text, given the parameters listed on top of the histograms. As *g* increases, the first peak separates from the main peak. This small first peak represents trials where the very first cells in the simulation receive damage but arrest for *g* generations and repair the damage. The trials in which the first cell dies immediately ('fraction zero') are not indicated in the histogram because the logarithm of zero is undefined, but the fraction is noted in each panel. The simulation was run for twenty generations $G = 20$ and repeated 10^4 times.

two progeny that survives, in agreement with experimental data for DSBs[100], or always both progeny that survive. This assumption can be removed in the theory by introducing parameters for the relative likelihoods that one offspring survives versus both offspring survive.

Timer strategy

A simple checkpoint strategy could be to wait for a fixed time t', and then advance with the cell cycle. Mathematically, this means setting $a(t | \{t_i\}) = \delta(t - t')$:

$$f(t') = e^{-t'/\tau} \int_0^\infty \prod_{E=1}^{E_0} dt_E \, r(\{t_i\}) \, s(t' | \{t_i\}) \quad . \tag{S2}$$

Assuming that each error is repaired independently according to the cumulative probability function $\rho(t_i)$ and each unrepaired error reduces the probability of survival by a factor σ, we obtain:

$$
\begin{aligned}
f(t') &= e^{-t'/\tau} \sum_{E=0}^{E_0} \binom{E_0}{E} \rho^{E_0-E}(t') \left(1 - \rho(t')\right)^E 1^{E_0-E} \sigma^E \\
&= e^{-t'/\tau} \left[\rho(t') + \sigma(1 - \rho(t')) \right]^{E_0} \\
&= e^{-t'/\tau} \left[\rho(t')(1-\sigma) + \sigma \right]^{E_0}
\end{aligned}
\tag{S3}
$$

The best timer strategy is obtained by maximizing $f(t')$ with respect to t',

$$
\tau E_0 \frac{\partial_{t'*} \rho(t'^*)}{\rho(t'^*) + \frac{\sigma}{1-\sigma}} = 1 \quad .
\tag{S4}
$$

Assuming that repairs follow a Poisson process, $\rho(t_i) = \rho_{\max}\left(1 - e^{-t_i/\tau_r}\right)$, we obtain for the optimal waiting time in the timer model:

$$
\frac{t'^*}{\tau_r} = \log \frac{1 + E_0 \frac{\tau}{\tau_r}}{1 + \frac{1}{\rho_{\max}}\frac{\sigma}{1-\sigma}} \quad ,
\tag{S5}
$$

which implies that unless

$$
E_0 \frac{\tau}{\tau_r} > \frac{1}{\rho_{\max}}\frac{\sigma}{1-\sigma}
\tag{S6}
$$

is satisfied, it is not worth waiting a fixed time for repair at a checkpoint at all ($t'^* = 0$), for example, if survival is too likely (σ close to 1).

Repair-threshold strategy

In an alternative model, a fixed amount $\left(E_0 - E'\right)$ of the total damage (E_0) is repaired before continuing with the cell cycle. Here,

$$
a(t|\{t_i\}) = \sum_{\text{perm.}} \underbrace{\delta(t - t_{i_1})}_{\text{1 repaired at } t} \underbrace{\theta(t - t_{i_2})\cdots\theta(t - t_{i_{E_0-E'}})}_{E_0-E'-1 \text{ repaired before } t} \underbrace{\theta(t_{i_{E_0-E'+1}} - t)\cdots\theta(t_{i_{E_0}} - t)}_{E' \text{ errors remaining}} \quad ,
\tag{S7}
$$

the cell cycle advancement probability, is equal to the sum of all permutations where damage i_1 is repaired at time t, before which $E_0 - E' - 1$ errors were repaired, leaving E' errors unrepaired.

Assuming as above that repair events are independent and survival for each error that remains at override is reduced by a factor σ, we obtain:

$$f(E') = \int_0^\infty dt\, E_0 \frac{d\rho(t)}{dt} \binom{E_0 - 1}{E'} \rho^{E_0 - E' - 1}(t)(1 - \rho(t))^{E'} \sigma^{E'} e^{-t/\tau} \quad . \tag{S8}$$

Assuming a Poisson process as above but with $\rho_M = 1$ to simplify the equations, we obtain:

$$f(E') = \frac{E_0!(E' + \tau_r/\tau)!}{(E_0 + \tau_r/\tau)!E'!} \sigma^{E'} \quad . \tag{S9}$$

Maximizing $f(E')$ with respect to E', we obtain:

$$\psi_0(1 + E'^* + \tau_r/\tau) - \psi_0(1 + E'^*) = -\log \sigma \quad , \tag{S10}$$

where ψ_0 is the polygamma function of order zero.

The left-hand side is a decreasing function of E'^*, so the larger the survival probability σ, the more errors E'^* can be tolerated for proceeding with the cell cycle.

E'^* is generally not an integer, and, therefore, $f(E'^*)$ has to be evaluated at the two nearest integers to E'^* to find the maximally tolerable amount of damage.

Optimal strategy is deterministic

The idea of the proof is as follows: To evaluate whether the optimal checkpoint strategy is stochastic or deterministic, we take a particular checkpoint strategy and increase or decrease the advancement probability $a(t, \{t_i\})$ at one point $(t, \{t_i\})$ in that strategy. Since the advancement probability must be normalized, that is, the integral or sum over all advancement probabilities must be equal to one, we also multiply all the other advancement probabilities that branch off from that point and that describe future advancement decisions by a compensatory factor. While satisfying the normalization constraint, we show that the fitness

coefficient of the strategy $f[a]$ can be increased unless the advancement probability density at that point was zero or infinity, that is, a Dirac delta (δ) function. A Dirac delta (δ) function advancement probability means that the checkpoint strategy is deterministic. Thus, only a deterministic strategy can be optimal.

To begin the proof, we assume that time is discretized with time points spaced Δt apart to replace integrals by sums. Consider a checkpoint strategy with advancement probability $a(t, \{t_i\})$ and a particular point in the strategy, that is, a damaged cell is arrested for time t, has $E(t)$ errors, and has repaired $E_0 - E(t)$ errors at times $\{t_j\}$ which are smaller than t. The value of $a(t | \{t_i\})$ of course only depends on t and the values of the repair times $\{t_j\}$ before t, since the repair times greater than t lie in the future. Therefore, $a(t | \{t_i\}) = a(t | \{t_j\})$ holds. The contribution of this advancement probability to the fitness coefficient is:

$$\Delta f_{\text{point}} = \Delta t \, r(\{t_i\}) s(t | \{t_i\}) a(t | \{t_i\}) e^{-t/\tau} \quad , \tag{S11}$$

according to Eq. (2.1).

Next, we consider the later advancement probabilities $a(t' | \{t_i'\})$ where $t' > t$ in which additional errors may have been repaired after t (the repaired errors before t are obviously the same $\{t_j\}$), see Fig. S2 for an illustration. These advancement probabilities make the following contributions to the fitness coefficient:

$$\Delta f_{\text{branch}} = \Delta t \sum_{t'} r(\{t_i'\}) s(t' | \{t_i'\}) a(t' | \{t_i'\}) e^{-t'/\tau} . \tag{S12}$$

Suppose that the advancement probabilities of the checkpoint strategy are normalized such that:

$$\text{const.} = a(t | \{t_i\}) + \sum_{t'} a(t' | \{t_i'\}). \tag{S13}$$

We create a new strategy in which we multiply $a(t | \{t_i\})$ by a factor α, yielding $\alpha a(t | \{t_i\})$, and we also multiply each of the later advancement probabilities $a(t' | \{t_i'\})$ by α':

$$\alpha' = 1 + (1 - \alpha) \frac{a(t | \{t_i\})}{\sum_{t'} a(t' | \{t_i'\})} \quad . \tag{S14}$$
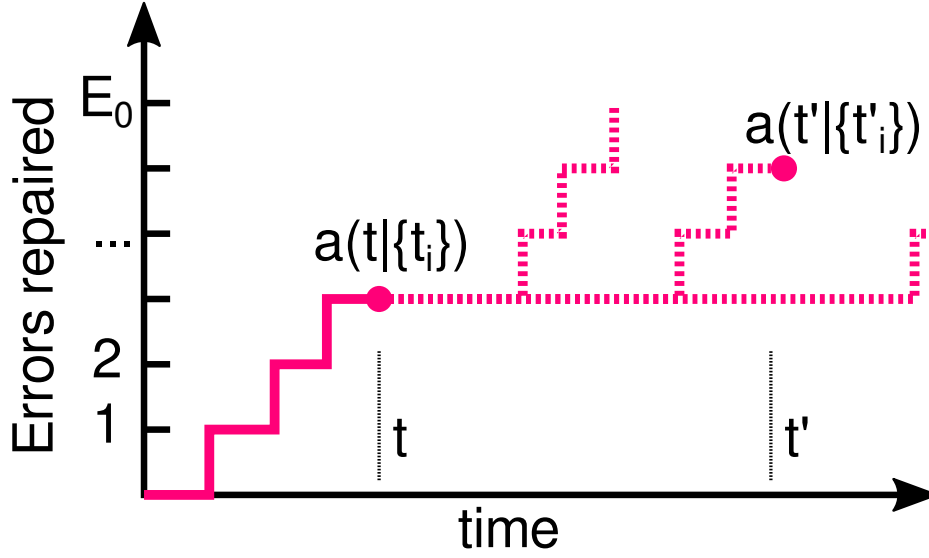
Fig. S2 – Illustration of trajectories in a checkpoint strategy. Solid lines indicate the realized trajectory (sequence of repairs) of the cell until time t. Dashed lines indicate possible future trajectories. The advancement probabilities $a(t|\{t_i\})$ at time t and $a(t'|\{t_i'\})$ at a later time t' are indicated.

We see that in the new checkpoint strategy,

$$\text{const.} = \alpha a(t|\{t_i\}) + \sum_{t'} \alpha' a(t'|\{t_i'\}) \quad , \tag{S15}$$

the advancement probability continues to be correctly normalized.

Plugging in the scaled advancement probabilities, we see that in this new strategy, the modified point contributes:

$$\alpha \Delta f_{\text{point}} = \alpha \Delta t \, r(\{t_i\}) s(t|\{t_i\}) a(t|\{t_i\}) e^{-t/\tau} \tag{S16}$$

to the fitness coefficient and the contribution of the future points is:

$$
\begin{aligned}
\alpha' \Delta f_{\text{branch}} &= \alpha' \Delta t \sum_{t'} r(\{t_i'\}) s(t'|\{t_i'\}) a(t'|\{t_i'\}) e^{-t'/\tau}, \\
&= \left[1 + (1-\alpha) \frac{a(t|\{t_i\})}{\sum_{t'} a(t'|\{t_i'\})} \right] \Delta t \sum_{t'} r(\{t_i'\}) s(t'|\{t_i'\}) a(t'|\{t_i'\}) e^{-t'/\tau} \quad ,
\end{aligned}
\tag{S17}
$$

which is linear in α. Since the contributions to the fitness coefficient are linearly dependent

on the parameter α,

$$\alpha \Delta f_{\text{point}} + \alpha' \Delta f_{\text{branch}} = O(\alpha^0) + \alpha \Delta t \, a(t|\{t_i\})$$

$$\times \left[r(\{t_i\}) s(t|\{t_i\}) e^{-t/\tau} - \sum_{t'} r(\{t_i'\}) s(t'|\{t_i'\}) e^{-t'/\tau} \frac{a(t'|\{t_i'\})}{\sum_{t''} a(t''|\{t_i''\})} \right]$$

$$\tag{S18}$$

the fitness coefficient of this strategy could not be maximal, unless either $a(t|\{t_i\})$ is zero or all future $a(t'|\{t_i'\})$ are zero. (Here, we assume that the slope of α, which is proportional to the term in square brackets in Eq. (S18), is not zero. This term is the difference between the contribution to the fitness coefficient if the advancement took place at t and the average contributions of all future divisions, which are weighted by their conditional advancement probability $\frac{a(t'|\{t_i'\})}{\sum_{t''} a(t''|\{t_i''\})}$. Generically, it will not be zero.)

This argument applies for every point in the error-time plane, such that at points where $\Delta t \, a(t, \{t_i\})$ is nonzero, it must be equal to one. In the limit $\Delta t \to 0$ as the discretization becomes smaller, $a(t, \{t_i\})$ becomes a Dirac delta (δ) function.

Additional information regarding the optimal strategy

Here, we provide additional details for Step 2 (main text) for computing the optimal strategy and describe Steps 3-5 depicted in Fig. 2.3 D-F.

2. First, we provide more information regarding Step 2 in the main text. Equating the two terms discussed in Step 2, $\frac{dt\partial_t \rho}{1-\rho} E\left(s(E-1) - s(E)\right) e^{-t/\tau}$ and $-s(E) dt \partial_t e^{-t/\tau}$, we obtain,

$$\frac{\partial_t \rho}{1-\rho}\bigg|_{t=t_{E,r}^*} \tau E\left(\frac{s(E-1)}{s(E)} - 1\right) = 1 \quad. \tag{S19}$$

Next, we use $s(E) = \sigma^E$ and only keep the linear term in σ, neglecting the $O(\sigma^2)$ terms. This is justified, for example, for an unrepaired DSB since the survival probability is very small ($\sigma \ll 1$) (Fig. 2.7 D). This yields Eq. (2.2).

3. For the left advancement boundary at each E, we need to compare the instantaneous fitness $s(E) e^{-t/\tau}$ with the expected future fitness. To calculate the expected number

of progeny due to waiting, one needs to take into account the possibility that another repair happens before reaching the right boundary at $t_{E,\mathrm{r}}^*$ versus the possibility that no other such repair occurs (Fig. 2.3 D). This leads to the following condition:

$$
\begin{aligned}
s(E)e^{-t_{E,\ell}^*/\tau} = &\int_{t_{E,\ell}^*}^{t_{E,\mathrm{r}}^*} dt'\,(-\partial_{t'}) \left[\frac{1-\rho(t')}{1-\rho(t_{E,\ell}^*)} \right]^E s(E-1)e^{-t'/\tau} \\
&+ \left[\frac{1-\rho(t_{E,\mathrm{r}}^*)}{1-\rho(t_{E,\ell}^*)} \right]^E s(E)e^{-t_{E,\mathrm{r}}^*/\tau} \quad .
\end{aligned}
\tag{S20}
$$

This sets the left advancement boundary $t_{E,\ell}^*$ at E (Fig. 2.3 E). (The last two equations are related; Eq. (S20) simplifies to Eq. (S19) by taking the derivative with respect to $t_{E,\mathrm{r}}^*$ and setting $t_{E,\ell}^* = t_{E,\mathrm{r}}^*$.)

4. It is, in principle, possible for there to be alternating segments of advancement boundary and waiting episodes (Fig. S3 A). Additional boundary points, if they exist, can be found by solving for the right-most $t_{E,\mathrm{r}}^*$, then the preceding $t_{E,\ell}^*$, and then for a possible right boundary further to the left and so on.

5. Thus far, all calculations assumed that with one fewer error $(E-1)$, it is optimal to advance and that there is a continuous advancement boundary line, as for $E = 0$. This assumption explicitly entered the right-hand sides of Eqns. 2.2, S19, and S20 which refer to the survival probability if one more error is fixed $(s(E-1))$ at the advancement boundary at $E-1$. However, if at the previous step, which means at some time point t and for $E-1$ errors, the optimal decision is to wait, it would not be correct to assess the consequence of reaching that point by the survival probability $s(E-1)$ since upon arriving at t and $E-1$, the cell cycle should continue to arrest. So, to calculate the optimal checkpoint decision for $E+1$ errors after the advancement boundary for E has been computed, for all times between the advancement boundaries, e.g., between $t_{E,\ell}^*$ and $t_{E,\mathrm{r}}^*$ in Fig. 2.3 F, the expected number of offspring $f_{\mathrm{wait}}(t, E)$ needs to be computed. The formula for $f_{\mathrm{wait}}(t, E)$ has to be adapted to the specific situation but can be based

on the following example:

$$f_{\text{wait}}(t, E) = \int_t^{t_{E,\text{r}}^*} dt' \, (-\partial_{t'}) \left[\frac{1 - \rho(t')}{1 - \rho(t)} \right]^E f_{\text{wait}}(t', E-1) e^{(t-t')/\tau}$$
$$+ \left[\frac{1 - \rho(t_{E,\text{r}}^*)}{1 - \rho(t)} \right]^E s(E) e^{(t-t_{E,\text{r}}^*)/\tau} \quad , \tag{S21}$$

which describes a strategy in which the cell will wait at $E - 1$ (because there is also a $f_{\text{wait}}(t', E - 1)$ term on the right-hand side). $f_{\text{wait}}(t, E)$ replaces $s(E)$ in the above formulas for calculating the advancement boundary for $E + 1$ errors (Fig. S3 B).
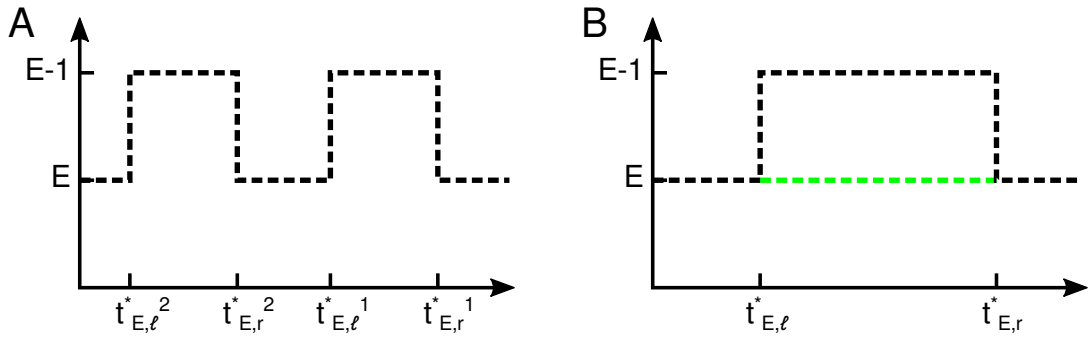
Fig. S3 – Additional plots to illustrate the recursive solution to the checkpoint optimization problem. A: Boundary with alternating advancement boundaries ($t_{E,\text{r}}^{*,i+1}$ to $t_{E,\ell}^{*,i}$) and wait segments ($t_{E,\ell}^{*,i}$ to $t_{E,\text{r}}^{*,i}$). B: After all points for E have been analyzed, there are either advancement segments (black) or wait segments (green) with the expected numbers of progeny computed at each point of the wait segments. The calculations can then be repeated for $E + 1$ errors.

For a Poisson process $\rho(t) = 1 - e^{-t/\tau_r}$, one can see by plugging into Eq. (2.2) that the boundaries are always horizontal, thus the optimal strategy reduces to the repair-threshold strategy. (The resulting condition, $\tau/\tau_r D(1/\sigma - 1) = 1$, is not obviously equivalent to Eq. (S10), but we checked numerically, scanning a large range of parameters, that they both give the same optimal horizontal boundary.)

2.6.2 Supplementary experimental results
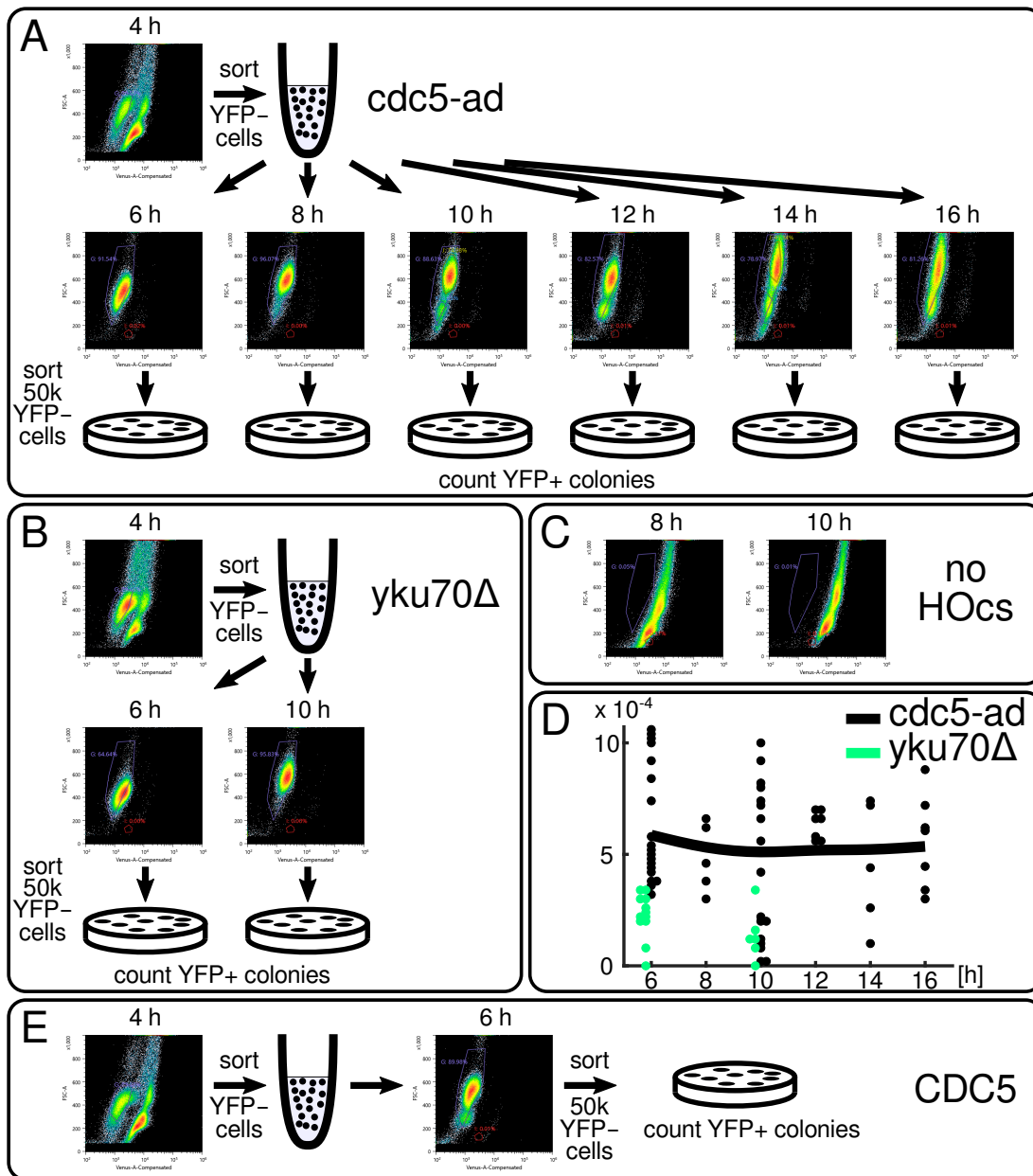
Fig. S4 – Supplementary data for the FACS experiments. A-C, E: FACS gates and protocols for the indicated strains. D: Total fraction of colonies (YFP- and YFP+ together) relative to 50 000 YFP- cells that were plated. Same experiments as shown in Fig. 2.6 B but only the fraction of YFP+ colonies is shown in Fig. 2.6 B.
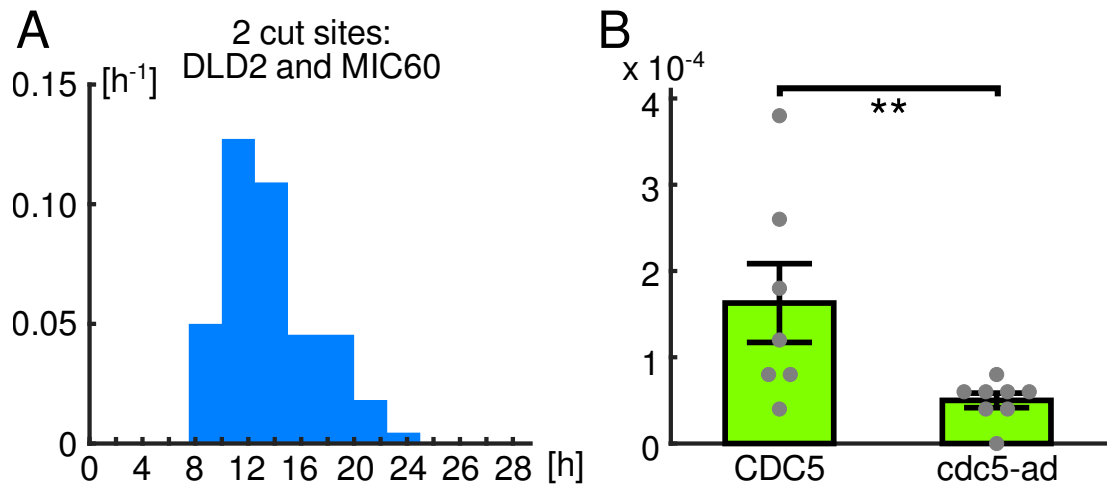
Fig. S5 – A: Histogram of budding-to-nuclear-division probabilities for cells with the two cut sites indicated. n = 88. Figure related to Fig. 2.7. B: Checkpoint override is an advantageous strategy, as determined by a direct comparison of survival probabilities for override-performing (*CDC5*) versus override-unable (*cdc5-ad*) cells. Each grey circle represents the fraction of YFP+ colonies emerging after sorting for 50 000 YFP- cells at the 6 h time point, and plating on Glu-Met medium plates. Mean ± SEM shown. p = 0.0075, one-tailed. n = 7 (*CDC5*), 8 (*cdc5-ad*).

2.6.3 Supplementary note: Further applications

To facilitate further applications of the optimal checkpoint theory, we discuss here steps to using the theory in other systems.

- The spindle assembly checkpoint has been measured to override after 120 min in budding yeast in the continued presence of the microtubule-depolarizing agent nocodazole,[76] which does not allow the number of errors to be controlled accurately. The activity of elements of the checkpoint can be monitored during nuclear division by Mad2-GFP localization[76], potentially obviating the need for override-suppressing mutations such as *cdc5-ad*; overriding cells are identifiable in post-processing[76]. To measure repair statistics and survival statistics, nocodazole exposure can be withdrawn by washing it out. Instead of drugs, more precise control can in principle be exerted over the numbers and timing of errors by way of inducible suppression of specific centromeres,[101] in analogy to the controlled generation of DSBs.

- In response to injury, checkpoints arrest insect development, and some of these checkpoints have been shown to be overridden if the damage is not repaired.[4] *Drosophila* larvae delay entry into pupariation if their imaginal discs are damaged at specific developmental stages; this delay is thought to allow for regeneration but is limited even if the damage is not repaired, e.g., to $\approx$40 hrs under the experimental conditions in ref.[17] All three quantities of the checkpoint theory can be measured with current technology[17,18]: repair statistics (fraction of adult flies capable of flight as a function of developmental delay), survival statistics (fraction of flies capable of flight if the checkpoint was overridden), and override times. Similar to our DNA break experiments, damage can be induced for a short time window or continuously.[17,18] Suppression of checkpoint override as with the *cdc5-ad* mutation in yeast may not be needed if the fates of pre-override and post-override animals[17,18] are sufficiently distinct.

- Checkpoint adaptation is believed to be associated with cancer emergence or exacerbation in human cells.[5] Tumor-derived U2OS cells arrest in response to ionizing irradiation and are reported to override the DNA damage checkpoint.[16] The appropriate candidate for testing the optimal checkpoint theory may indeed be cells that are already cancerous

because they explore growth and presumably checkpoint strategies in competition with other cells.[53] The simplest prediction of the theory is that the cells' DNA damage checkpoint is neither absent nor strict, but overridable, as reported for various cell lines.[5] Another relatively simple test is whether different cancer cell lines show similar arrest times in response to errors, suggesting the presence of an optimal strategy and an optimal arrest time. Similar to other cases, the transfer of experiments from yeast to mammalian cells is in principle possible, but will require further developments in technology such as inducible CRISPR-Cas9 systems that are proven to not interfere with post-break DNA repair.

3 Conclusions

Checkpoints are critical for living systems. However, they are poorly characterized quantitatively by experiment or theory. In particular, checkpoint override is an inherently quantitative phenomenon that invites an organism-level analysis, which had not been carried out previously. In my work, I sought to advance this understanding of checkpoints.

Despite high levels of noise, we found that DNA damage checkpoint override follows predictable patterns. We discovered these timing hierarchies following the predictions of our theory.

The fundamental idea, which we relied on to develop the theory, was the principle of offspring maximization; different population genetics models showed that the quantity that evolution should be expected to have maximized is the probability of producing live progeny multiplied by an exponential time penalty for arrest. Three well-known models of population genetics, involving exponential growth or fixed-size populations (Wright-Fisher and Moran models), were drawn on in this analysis. In reality, fitness maximization would have been performed by natural selection: If two strategies existed in a population of cells, the one closer to the optimum ought to have won out over evolutionary timescales – until an even more optimal strategy would appear and win out.

The results of our analysis are general because they describe a fundamental balance between risk, represented by repair and survival probabilities, and growth. Thus, other biological surveillance systems could be investigated with regard to their balances on the basis of our

theory.

Interestingly, a deterministic strategy turned out to be optimal. Experimentally, however, the observed distributions of checkpoint override times (Fig. 2.5 B) were broad. This discrepancy remains a topic for future study. In fact, other authors have suggested that fluctuating environments could cause a stochastic strategy to be more advantageous than a deterministic strategy.[102]

The general fitness functional (Eq. (2.1)) served to prove that the optimal strategy is deterministic. This allowed us to map the problem of maximizing the fitness functional onto the question of finding the optimal boundary for a random walk. We found that this problem allowed closed-form recursive solutions. Simulations were not needed to solve the equations.

There are three independent quantities, i) the probability distribution of error correction, ii) the survival probability if errors are not fixed, and iii) the optimal timing of checkpoint override, which the theory relates to each other. After providing experimental values for i) and ii), the theory predicted iii), the override time as a function of the number of errors.

In our experiments, we focused on budding yeast and on the DNA damage checkpoint because it was relatively well explored by molecular geneticists. We built a budding yeast system whose cell cycle stage could be controlled, a specific number of DSBs could be induced, and the cells with DSBs could be separated from intact cells based on the fluorescence output of the DSB sensor. This system allowed us to eliminate repaired cells by flow cytometry and capture rare repair events.

Using this experimental system, we were able to measure the parameters of the theory and the predictions precisely. The predictions matched the observations well. It is important to note that the predictions and experimental data were non-trivial: The override times varied by finite amounts as a function of the number of DSBs. These finite shifts were predicted well by the theory.

Interestingly, the theoretical predictions compelled us to reexamine the current view in the field[29,31,33] that override only occurs for 1 DSB and not 2 Ho-induced DSBs[27], which implied that checkpoint override is limited and not a universal response to DNA damage in wild-

type cells. Instead, we found override to occur with up to 4 DSBs. This result brings the observations about DNA damage checkpoint override more in line with each other since the failure to override with 2 DSBs stands out from the other results. For example, override has been documented with plausibly large amounts of DNA damage due to X-rays[28] or telomere dysfunction in *cdc13-1*[2] or *tlc1Δ*[29] cells. It is no longer necessary to explain these differences by postulating that different types of DSBs must have different effects on override.[33]

The result of Lee et al. that the DNA damage checkpoint does not override with 2 DSBs supported a molecular model in which the amount of post-break DNA resection determines whether or not override occurs.[27] Presumably, the threshold on resected ssDNA allowing or blocking override would be between the amount produced in response to 1 to 2 DSBs. However, the model was already challenged by the discovery of mutants that produce less post-break DNA resection but also did not override.[31] In principle, this model can be modified to be consistent with our data: increasing amounts of ssDNA due to additional breaks simply increase the arrest duration by finite amounts.

Finally, we demonstrated the biological relevance of checkpoint override – without crippling DNA repair or maintenance. This was made possible with our DNA damage sensor. It allowed us to select only cells that had not repaired their DSB for many hours after break induction and compare override-blocked (*cdc5-ad*) and override-competent (*CDC5*) cells.

The field of checkpoint biology is largely driven by molecular genetics. Our quantitative, system-level study complements these efforts and ought to help drive them forward. A key central question will be how the override computation is performed dynamically by the complex DNA damage checkpoint machinery, which involves *CDC5*[2], *RAD53*[34], *PTC2* and *PTC3*[30], and other genes[6,31]. The global, system-level analysis that we provided ought to guide and constrain the molecular exploration of this complex system.

4 Future work

There are, in principle, four important directions for future research: i) elucidating the biological function of override of the DNA damage checkpoint, ii) dissecting how the DNA damage checkpoint computes override times, iii) identifying the signal that is read out for setting the DNA damage checkpoint override time, and iv) testing the theory in other systems.

While we showed that DDC override is beneficial for survival for yeast cells with 1 double-strand DNA break (DSB), and that there are temporal patterns underlying how the DDC overrides (8 hrs for 1 DSB, 14 hrs for 2 DSBs, ...), the mechanism that renders override advantageous and the biological significance of the striking override time pattern remain unknown. Using dynamic perturbations and single-cell readout, one should examine i) the mechanisms increasing survival rates after override and ii) the importance of override timing for cell fitness, tested by varying the time experimentally. Explaining the function of override ought to motivate research into other systems where override may also create a fitness advantage, e.g., cancer cells.

We have shown that cells adjust override times to the amount of damage gradually and dynamically. However, we do not know how DNA damage checkpoint proteins interact dynamically to trigger override. Focusing on the central genes involved in override, one should manipulate the level of each and the time at which each increases. One should measure the impact of these changes in single cells in order to deduce the molecular mechanisms that determine override timing. Past research has uncovered many genes and interactions but a

dynamic, circuit-level model is missing.

We found that the override time changes dynamically with the number of DSBs. Whether the number of DNA ends or resected ssDNA determine the override time is a fundamental but open question. Newer data call into question[6] the well-known model[27] that DNA resection sets override times. Combining novel 'resection sensors' developed by us with known resection rate mutations, one should establish the relationship between the number of DNA ends, ssDNA, and override times at the single-cell level. How cells measure damage to set the arrest time has been researched intensely but has remained elusive.

Theory can compel new kinds of experiments to uncover previously hidden patterns. A powerful aspect of a general, first-principles theory is that it can apply to disparate systems. We envisage a number of further applications. The spindle assembly checkpoint (SAC) has been measured to override after 120 min in budding yeast in the continued presence of the microtubule-depolarizing agent nocodazole,[76] which does not allow the number of errors to be controlled accurately. The activity of elements of the checkpoint can be monitored during nuclear division by Mad2-GFP localization[76], potentially obviating the need for override-suppressing mutations such as *cdc5-ad*; overriding cells are identifiable in post-processing[76]. To measure repair statistics and survival statistics, nocodazole exposure can be withdrawn by washing it out. A second potential application is in developmental biology. In response to injury, checkpoints arrest insect development, and some of these checkpoints have been shown to be overridden if the damage is not repaired.[4] *Drosophila* larvae delay entry into pupariation if their imaginal discs are damaged at specific developmental stages; this delay is thought to allow for regeneration but is limited even if the damage is not repaired, e.g., to ≈40 hrs under the experimental conditions in ref.[17] All three quantities of the checkpoint theory can be measured with current technology[17,18]: repair statistics (fraction of adult flies capable of flight as a function of developmental delay), survival statistics (fraction of flies capable of flight if the checkpoint was overridden), and override times. Similar to our DNA break experiments, damage can be induced for a short time window or continuously.[17,18] Suppression of checkpoint override as with the *cdc5-ad* mutation in yeast may not be needed if the fates of pre-override and post-override animals[17,18] are sufficiently distinct. Finally, checkpoint adaptation is believed to be associated with cancer emergence or exacerbation

in human cells.[5] Tumor-derived U2OS cells arrest in response to ionizing irradiation and are reported to override the DNA damage checkpoint.[16] The appropriate candidate for testing the optimal checkpoint theory may indeed be cells that are already cancerous because they explore growth and presumably checkpoint strategies in competition with other cells.[53] The simplest prediction of the theory is that the cells' DNA damage checkpoint is neither absent nor strict, but overridable, as reported for various cell lines.[5] Another relatively simple test is whether different cancer cell lines show similar arrest times in response to errors, suggesting the presence of an optimal strategy and an optimal arrest time. Similar to other cases, the transfer of experiments from yeast to mammalian cells is in principle possible, but will require further developments in technology such as inducible CRISPR-Cas9 systems that are proven to not interfere with post-break DNA repair.

The quantitative examination of the override of the DNA damage checkpoint, which I performed in my PhD studies, leads to further fundamental questions, for which the ideas, tools, and data that I generated ought to be very helpful.

Bibliography

1. Sandell, L. L. & Zakian, V. A. Loss of a yeast telomere: Arrest, recovery, and chromosome loss. *Cell* **75**, 729–739 (1993).

2. Toczyski, D. P., Galgoczy, D. J. & Hartwell, L. H. CDC5 and CKII control adaptation to the yeast DNA damage checkpoint. *Cell* **90**, 1097–1106 (1997).

3. Rieder, C. L. & Maiato, H. Stuck in division or passing through: What happens when cells cannot satisfy the spindle assembly checkpoint. *Dev. Cell* **7**, 637–651 (2004).

4. Hackney, J. F. & Cherbas, P. Injury response checkpoint and developmental timing in insects. *Fly* **8**, 226–231 (2014).

5. Swift, L. & Golsteyn, R. Chapter 22 - the relationship between checkpoint adaptation and mitotic catastrophe in genomic changes in cancer cells. In *Genome Stability* (eds. Kovalchuk, I. & Kovalchuk, O.), 373–389 (Academic Press, 2016).

6. Waterman, D. P., Haber, J. E. & Smolka, M. B. Checkpoint responses to DNA double-strand breaks. *Annu. Rev. Biochem.* **89**, 103–133 (2020).

7. Perkins, T. J. & Swain, P. S. Strategies for cellular decision-making. *Mol. Syst. Biol.* **5**, 326 (2009).

8. Alon, U. *An Introduction to Systems Biology: Design Principles of Biological Circuits* (Chapman & Hall/CRC, 2019).

9. Hartwell, L. & Weinert, T. Checkpoints: controls that ensure the order of cell cycle events. *Science* **246**, 629–634 (1989).

10. Elledge, S. J. Cell cycle checkpoints: Preventing an identity crisis. *Science* **274**, 1664–1672 (1996).

11. Zhou, B.-B. S. & Elledge, S. J. The DNA damage response: putting checkpoints in perspective. *Nature* **408**, 433–439 (2000).

Bibliography

12. Negrini, S., Gorgoulis, V. G. & Halazonetis, T. D. Genomic instability – an evolving hallmark of cancer. *Nat. Rev. Mol. Cell Biol.* **11**, 220–228 (2010).

13. Symington, L. S. & Gautier, J. Double-strand break end resection and repair pathway choice. *Annu. Rev. Genet.* **45**, 247–271 (2011). PMID: 21910633.

14. Kramara, J., Osia, B. & Malkova, A. Break-induced replication: The where, the why, and the how. *Trends Genet.* **34**, 518–531 (2018).

15. Rossio, V., Galati, E. & Piatti, S. Adapt or die: how eukaryotic cells respond to prolonged activation of the spindle assembly checkpoint. *Biochem. Soc. Trans.* **38**, 1645–1649 (2010).

16. Syljuåsen, R. G. Checkpoint adaptation in human cells. *Oncogene* **26**, 5833–5839 (2007).

17. Halme, A., Cheng, M. & Hariharan, I. K. Retinoids regulate a developmental checkpoint for tissue regeneration in drosophila. *Curr. Biol.* **20**, 458–463 (2010).

18. Hackney, J. F., Zolali-Meybodi, O. & Cherbas, P. Tissue damage disrupts developmental progression and ecdysteroid biosynthesis in *Drosophila*. *PLoS One* **7**, 1–12 (2012).

19. Wu, D., Topper, L. M. & Wilson, T. E. Recruitment and dissociation of nonhomologous end joining proteins at a DNA double-strand break in *Saccharomyces cerevisiae*. *Genetics* **178**, 1237–1249 (2008).

20. Balestrini, A., Ristic, D., Dionne, I., Liu, X. Z., Wyman, C., Wellinger, R. J. & Petrini, J. H. The Ku heterodimer and the metabolism of single-ended DNA double-strand breaks. *Cell Rep.* **3**, 2033–2045 (2013).

21. Chiruvella, K. K., Liang, Z., Birkeland, S. R., Basrur, V. & Wilson, T. E. *Saccharomyces cerevisiae* DNA ligase IV supports imprecise end joining independently of its catalytic activity. *PLoS Genet.* **9**, 1–12 (2013).

22. Liang, Z., Sunder, S., Nallasivam, S. & Wilson, T. E. Overhang polarity of chromosomal double-strand breaks impacts kinetics and fidelity of yeast non-homologous end joining. *Nucleic Acids Res.* **44**, 2769–2781 (2016).

23. Muñoz-Galván, S., López-Saavedra, A., Jackson, S. P., Huertas, P., Cortés-Ledesma, F. & Aguilera, A. Competing roles of DNA end resection and non-homologous end joining functions in the repair of replication-born double-strand breaks by sister-chromatid recombination. *Nucleic Acids Res.* **41**, 1669–1683 (2012).

24. Lisby, M., Mortensen, U. H. & Rothstein, R. Colocalization of multiple DNA double-strand breaks at a single Rad52 repair centre. *Nat. Cell Biol.* **5**, 572–577 (2003).

25. Seeber, A., Hauer, M. H. & Gasser, S. M. Chromosome dynamics in response to DNA damage. *Annu. Rev. Genet.* **52**, 295–319 (2018).

26. Waterman, D. P., Zhou, F., Li, K., Lee, C.-S., Tsabar, M., Eapen, V. V., Mazzella, A. & Haber, J. E. Live cell monitoring of double strand breaks in *S. cerevisiae. PLoS Genet.* **15**, 1–22 (2019).

27. Lee, S. E., Moore, J., Holmes, A., Umezu, K., Kolodner, R. D. & Haber, J. E. *Saccharomyces* Ku70, Mre11/Rad50, and RPA proteins regulate adaptation to G2/M arrest after DNA damage. *Cell* **94**, 399–409 (1998).

28. Galgoczy, D. J. & Toczyski, D. P. Checkpoint adaptation precedes spontaneous and damage-induced genomic instability in yeast. *Mol. Cell. Biol.* **21**, 1710–1718 (2001).

29. Coutelier, H., Xu, Z., Morisse, M. C., Lhuillier-Akakpo, M., Pelet, S., Charvin, G., Dubrana, K. & Teixeira, M. T. Adaptation to DNA damage checkpoint in senescent telomerase-negative cells promotes genome instability. *Genes Dev.* **32**, 1499–1513 (2018).

30. Leroy, C., Lee, S. E., Vaze, M. B., Ochsenbien, F., Guerois, R., Haber, J. E. & Marsolier-Kergoat, M.-C. PP2C phosphatases Ptc2 and Ptc3 are required for DNA checkpoint inactivation after a double-strand break. *Mol. Cell* **11**, 827–835 (2003).

31. Haber, J. E. A life investigating pathways that repair broken chromosomes. *Annu. Rev. Genet.* **50**, 1–28 (2016).

32. Lee, S. E., Pellicioli, A., Demeter, J., Vaze, M. P., Gasch, A. P., Malkova, A., Brown, P. O., Botstein, D., Stearns, T., Foiani, M. & Haber, J. E. Arrest, adaptation, and recovery following a chromosome double-strand break in *Saccharomyces cerevisiae. Cold Spring Harb. Symp. Quant. Biol.* **65**, 303–314 (2000).

33. Coutelier, H. & Xu, Z. Adaptation in replicative senescence: a risky business. *Curr. Genet.* **65**, 711–716 (2019).

34. Pellicioli, A., Lee, S. E., Lucca, C., Foiani, M. & Haber, J. E. Regulation of *Saccharomyces* Rad53 checkpoint kinase during adaptation from DNA damage–induced G2/M arrest. *Mol. Cell* **7**, 293–300 (2001).

35. Guillemain, G., Ma, E., Mauger, S., Miron, S., Thai, R., Guérois, R., Ochsenbein, F. & Marsolier-Kergoat, M.-C. Mechanisms of checkpoint kinase Rad53 inactivation after a double-strand break in *Saccharomyces cerevisiae. Mol. Cell. Biol.* **27**, 3378–3389 (2007).

36. Memisoglu, G., Eapen, V. V., Yang, Y., Klionsky, D. J. & Haber, J. E. PP2C phosphatases

promote autophagy by dephosphorylation of the Atg1 complex. *Proc. Natl. Acad. Sci. U. S. A.* **116**, 1613–1620 (2019).

37. Lee, S. E., Pellicioli, A., Vaze, M. B., Sugawara, N., Malkova, A., Foiani, M. & Haber, J. E. Yeast Rad52 and Rad51 recombination proteins define a second pathway of DNA damage assessment in response to a single double-strand break. *Mol. Cell. Biol.* **23**, 8913–8923 (2003).

38. Clerici, M., Mantiero, D., Lucchini, G. & Longhese, M. P. The *Saccharomyces cerevisiae* Sae2 protein negatively regulates DNA damage checkpoint signalling. *EMBO Rep.* **7**, 212–218 (2006).

39. Lee, S. E., Pellicioli, A., Malkova, A., Foiani, M. & Haber, J. E. The *Saccharomyces* recombination protein Tid1p is required for adaptation from G2/M arrest induced by a double-strand break. *Curr. Biol.* **11**, 1053–1057 (2001).

40. Eapen, V. V., Sugawara, N., Tsabar, M., Wu, W.-H. & Haber, J. E. The *Saccharomyces cerevisiae* chromatin remodeler Fun30 regulates DNA end resection and checkpoint deactivation. *Mol. Cell. Biol.* **32**, 4727–4740 (2012).

41. Dotiwala, F., Eapen, V. V., Harrison, J. C., Arbel-Eden, A., Ranade, V., Yoshida, S. & Haber, J. E. DNA damage checkpoint triggers autophagy to regulate the initiation of anaphase. *Proc. Natl. Acad. Sci. U. S. A.* **110**, E41–E49 (2013).

42. Gallina, I., Colding, C., Henriksen, P., Beli, P., Nakamura, K., Offman, J., Mathiasen, D. P., Silva, S., Hoffmann, E., Groth, A., Choudhary, C. & Lisby, M. Cmr1/WDR76 defines a nuclear genotoxic stress body linking genome integrity and protein quality control. *Nat. Commun.* **6**, 6533 (2015).

43. Clémenson, C. & Marsolier-Kergoat, M.-C. DNA damage checkpoint inactivation: Adaptation and recovery. *DNA Repair* **8**, 1101–1109 (2009). Checkpoint response to DNA damage.

44. Keogh, M.-C., Kim, J.-A., Downey, M., Fillingham, J., Chowdhury, D., Harrison, J. C., Onishi, M., Datta, N., Galicia, S., Emili, A., Lieberman, J., Shen, X., Buratowski, S., Haber, J. E., Durocher, D., Greenblatt, J. F. & Krogan, N. J. A phosphatase complex that dephosphorylates γH2AX regulates DNA damage checkpoint recovery. *Nature* **439**, 497–501 (2006).

45. Hustedt, N., Seeber, A., Sack, R., Tsai-Pflugfelder, M., Bhullar, B., Vlaming, H., van

Leeuwen, F., Guénolé, A., van Attikum, H., Srivas, R., Ideker, T., Shimada, K. & Gasser, S. M. Yeast PP4 interacts with ATR homolog Ddc2-Mec1 and regulates checkpoint signaling. *Molecular Cell* **57**, 273–289 (2015).

46. Vidanes, G. M., Sweeney, F. D., Galicia, S., Cheung, S., Doyle, J. P., Durocher, D. & Toczyski, D. P. CDC5 inhibits the hyperphosphorylation of the checkpoint kinase Rad53, leading to checkpoint adaptation. *PLoS Biol.* **8**, e1000286 (2010).

47. Donnianni, R. A., Ferrari, M., Lazzaro, F., Clerici, M., Tamilselvan Nachimuthu, B., Plevani, P., Muzi-Falconi, M. & Pellicioli, A. Elevated levels of the Polo kinase Cdc5 override the Mec1/ATR checkpoint in budding yeast by acting at different steps of the signaling pathway. *PLoS Genet.* **6**, 1–14 (2010).

48. Schleker, T., Shimada, K., Sack, R., Pike, B. L. & Gasser, S. M. Cell cycle-dependent phosphorylation of Rad53 kinase by Cdc5 and Cdc28 modulates checkpoint adaptation. *Cell cycle* **9**, 350–63 (2010).

49. Botchkarev, V. V. & Haber, J. E. Functions and regulation of the Polo-like kinase Cdc5 in the absence and presence of DNA damage. *Curr. Genet.* **64**, 87–96 (2018).

50. Jaehnig, E. J., Kuo, D., Hombauer, H., Ideker, T. G. & Kolodner, R. D. Checkpoint kinases regulate a global network of transcription factors in response to {DNA} damage. *Cell Rep.* **4**, 174–188 (2013).

51. Rossio, V., Galati, E. & Piatti, S. Adapt or die: how eukaryotic cells respond to prolonged activation of the spindle assembly checkpoint. *Biochem. Soc. Trans.* **38**, 1645–1649 (2010).

52. Sadeghi, A., Dervey, R., Gligorovski, V. & Rahi, S. J. The optimal checkpoint strategy balancing risk and speed predicts experimental DNA damage checkpoint override times. *bioRxiv* 2020.08.14.251504 (2020). In revision, Nature Physics, screenshot from submission web site attached as evidence. Preprint: https://doi.org/10.1101/2020.08.14.251504.

53. Bowling, S., Lawlor, K. & Rodríguez, T. A. Cell competition: the winners and losers of fitness selection. *Development* **146**, 1–12 (2019).

54. Jain, S., Sugawara, N., Lydeard, J., Vaze, M., Tanguy Le Gac, N. & Haber, J. E. A recombination execution checkpoint regulates the choice of homologous recombination pathway during DNA double-strand break repair. *Genes Dev.* **23**, 291–303 (2009).

55. Hopfield, J. J. Kinetic proofreading: A new mechanism for reducing errors in biosynthetic processes requiring high specificity. *Proc. Natl. Acad. Sci. U. S. A.* **71**, 4135–4139 (1974).

56. Ninio, J. Kinetic amplification of enzyme discrimination. *Biochimie* **57**, 587–595 (1975).

57. Berg, H. & Purcell, E. Physics of chemoreception. *Biophys. J.* **20**, 193–219 (1977).

58. Ehrenberg, M. & Blomberg, C. Thermodynamic constraints on kinetic proofreading in biosynthetic pathways. *Biophys. J.* **31**, 333–358 (1980).

59. Freter, R. R. & Savageau, M. A. Proofreading systems of multiple stages for improved accuracy of biological discrimination. *J. Theor. Biol.* **85**, 99–123 (1980).

60. Savageau, M. A. & Lapointe, D. S. Optimization of kinetic proofreading: A general method for derivation of the constraint relations and an exploration of a specific case. *J. Theor. Biol.* **93**, 157–177 (1981).

61. McKeithan, T. W. Kinetic proofreading in T-cell receptor signal transduction. *Proc. Natl. Acad. Sci. U. S. A.* **92**, 5042–5046 (1995).

62. Murugan, A., Huse, D. A. & Leibler, S. Speed, dissipation, and error in kinetic proofreading. *Proc. Natl. Acad. Sci. U. S. A.* **109**, 12034–12039 (2012).

63. Lan, G., Sartori, P., Neumann, S., Sourjik, V. & Tu, Y. The energy-speed-accuracy trade-off in sensory adaptation. *Nat. Phys.* **8**, 422–428 (2012).

64. Sartori, P., Granger, L., Lee, C. F. & Horowitz, J. M. Thermodynamic costs of information processing in sensory adaptation. *PLoS Comput. Biol.* **10**, 1–9 (2014).

65. Rao, R. & Peliti, L. Thermodynamics of accuracy in kinetic proofreading: dissipation and efficiency trade-offs. *J. Stat. Mech: Theory Exp.* **2015**, P06001 (2015).

66. ten Wolde, P. R., Becker, N. B., Ouldridge, T. E. & Mugler, A. Fundamental limits to cellular sensing. *J. Stat. Phys.* **162**, 1395–1424 (2016).

67. Banerjee, K., Kolomeisky, A. B. & Igoshin, O. A. Elucidating interplay of speed and accuracy in biological error correction. *Proc. Natl. Acad. Sci. U. S. A.* **114**, 5183–5188 (2017).

68. Cui, W. & Mehta, P. Identifying feasible operating regimes for early T-cell recognition: The speed, energy, accuracy trade-off in kinetic proofreading and adaptive sorting. *PLoS One* **13**, 1–16 (2018).

69. Wong, F., Amir, A. & Gunawardena, J. Energy-speed-accuracy relation in complex networks for biological discrimination. *Phys. Rev. E* **98**, 012420 (2018).

70. Mallory, J. D., Kolomeisky, A. B. & Igoshin, O. A. Trade-offs between error, speed, noise, and energy dissipation in biological processes with proofreading. *J. Phys. Chem. B* **123**,

4718–4725 (2019).

71. Morgan, D. O. *The cell cycle: Principles of control* (New Science Press, 2007).

72. Breivik, J. & Gaudernack, G. Resolving the evolutionary paradox of genetic instability: a cost–benefit analysis of DNA repair in changing environments. *FEBS Lett.* **563**, 7–12 (2004).

73. Komarova, N. L., Sadovsky, A. V. & Wan, F. Y. Selective pressures for and against genetic instability in cancer: a time-dependent problem. *J. R. Soc. Interface* **5**, 105–121 (2008).

74. Nik-Zainal, S. & Hall, B. A. Cellular survival over genomic perfection. *Science* **366**, 802–803 (2019).

75. Ciliberto, A., Novak, B. & Tyson, J. J. Mathematical model of the morphogenesis checkpoint in budding yeast. *J. Cell Biol.* **163**, 1243–1254 (2003).

76. Bonaiuti, P., Chiroli, E., Gross, F., Corno, A., Vernieri, C., Štefl, M., Cosentino Lagomarsino, M., Knop, M. & Ciliberto, A. Cells escape an operational mitotic checkpoint through a stochastic process. *Curr. Biol.* **28**, 28–37 (2018).

77. Aguda, B. D. A quantitative analysis of the kinetics of the G2 DNA damage checkpoint system. *Proc. Natl. Acad. Sci. U. S. A.* **96**, 11352–11357 (1999).

78. Gérard, C. & Goldbeter, A. Temporal self-organization of the cyclin/Cdk network driving the mammalian cell cycle. *Proc. Natl. Acad. Sci. U. S. A.* **106**, 21643–21648 (2009).

79. Qu, Z., Weiss, J. N. & MacLellan, W. R. Regulation of the mammalian cell cycle: a model of the G1-to-S transition. *Am. J. Physiol.* **284**, C349–C364 (2003).

80. Qu, Z., MacLellan, W. R. & Weiss, J. N. Dynamics of the cell cycle: Checkpoints, sizers, and timers. *Biophys. J.* **85**, 3600–3611 (2003).

81. Iwamoto, K., Hamada, H., Eguchi, Y. & Okamoto, M. Mathematical modeling of cell cycle regulation in response to DNA damage: Exploring mechanisms of cell-fate determination. *Biosystems* **103**, 384–391 (2011).

82. He, E., Kapuy, O., Oliveira, R. A., Uhlmann, F., Tyson, J. J. & Novák, B. System-level feedbacks make the anaphase switch irreversible. *Proc. Natl. Acad. Sci. U. S. A.* **108**, 10016–10021 (2011).

83. Kesseler, K. J., Blinov, M. L., Elston, T. C., Kaufmann, W. K. & Simpson, D. A. A predictive mathematical model of the DNA damage G2 checkpoint. *J. Theor. Biol.* **320**, 159–169 (2013).

Bibliography

84. Iwamoto, K., Hamada, H., Eguchi, Y. & Okamoto, M. Stochasticity of intranuclear biochemical reaction processes controls the final decision of cell fate associated with DNA damage. *PLoS One* **9**, 1–12 (2014).

85. Heldt, F. S., Barr, A. R., Cooper, S., Bakal, C. & Novák, B. A comprehensive model for the proliferation–quiescence decision in response to endogenous DNA damage in human cells. *Proc. Natl. Acad. Sci. U. S. A.* **115**, 2532–2537 (2018).

86. Jung, Y. & Kraikivski, P. Computational model of G2-M DNA damage checkpoint regulation in normal and p53-null cancer cells. *bioRxiv* 2020.06.17.158246 (2020).

87. Chen, K. C., Calzone, L., Csikasz-Nagy, A., Cross, F. R., Novak, B. & Tyson, J. J. Integrative analysis of cell cycle control in budding yeast. *Mol. Biol. Cell* **15**, 3841–3862 (2004).

88. Curtis, N. L., Ruda, G. F., Brennan, P. & Bolanos-Garcia, V. M. Deregulation of chromosome segregation and cancer. *Annu. Rev. Cancer Biol.* **4**, 257–278 (2020).

89. Lee, S. E., Pâques, F., Sylvan, J. & Haber, J. E. Role of yeast SIR genes and mating type in directing DNA double-strand breaks to homologous and non-homologous repair paths. *Curr. Biol.* **9**, 767–770 (1999).

90. Chiruvella, K. K., Liang, Z. & Wilson, T. E. Repair of double-strand breaks by end joining. *Cold Spring Harbor Perspect. Biol.* **5**, a012757 (2013).

91. Crow, J. F. & Kimura, M. *An Introduction to Population Genetics Theory* (The Blackburn Press, 1970).

92. Orr, H. A. Fitness and its role in evolutionary genetics. *Nat. Rev. Genet.* **10**, 531–539 (2009).

93. Kelly Jr., J. L. A new interpretation of information rate. *Bell Syst. Tech. J.* **35**, 917–926 (1956).

94. Amon, A., Irniger, S. & Nasmyth, K. Closing the cell cycle circle in yeast: G2 cyclin proteolysis initiated at mitosis persists until the activation of G1 cyclins in the next cycle. *Cell* **77**, 1037 – 1050 (1994).

95. Dietler, N., Minder, M., Gligorovski, V., Economou, A. M., Joly, D. A. H. L., Sadeghi, A., Chan, C. H. M., Koziński, M., Weigert, M., Bitbol, A.-F. & Rahi, S. J. A convolutional neural network segments yeast microscopy images with high accuracy. *Nat. Commun.* **11**, 5723 (2020).

96. Kaboli, S., Yamakawa, T., Sunada, K., Takagaki, T., Sasano, Y., Sugiyama, M., Kaneko, Y.

& Harashima, S. Genome-wide mapping of unexplored essential regions in the *Saccharomyces cerevisiae* genome: evidence for hidden synthetic lethal combinations in a genetic interaction network. *Nucleic Acids Res.* **42**, 9838–9853 (2014).

97. Moore, J. K. & Haber, J. E. Cell cycle and genetic requirements of two pathways of nonhomologous end-joining repair of double-strand breaks in *Saccharomyces cerevisiae*. *Mol. Cell. Biol.* **16**, 2164–2173 (1996).

98. Haber, J. E. Mating-type genes and MAT switching in *Saccharomyces cerevisiae*. *Genetics* **191**, 33–64 (2012).

99. Elserafy, M. & El-Khamisy, S. F. Choose your yeast strain carefully: the RAD5 gene matters. *Nat. Rev. Mol. Cell Biol.* **19**, 343–344 (2018).

100. Kaye, J. A., Melo, J. A., Cheung, S. K., Vaze, M. B., Haber, J. E. & Toczyski, D. P. DNA breaks promote genomic instability by impeding proper chromosome segregation. *Curr. Biol.* **14**, 2096–2106 (2004).

101. Tsabar, M., Haase, J., Harrison, B., Snider, C. E., Eldridge, B., Kaminsky, L., Hine, R. M., Haber, J. E. & Bloom, K. A cohesin-based partitioning mechanism revealed upon transcriptional inactivation of centromere. *PLoS Genet.* **12**, 1–25 (2016).

102. Roux, P., Salort, D. & Xu, Z. Adaptation to DNA damage as a bet-hedging mechanism in a fluctuating environment. *R. Soc. Open Sci.* **8**, 210460 (2021).

Ahmad Sadeghi

ahmadsadeghi23@gmail.com

Contact

Website: https://www.epfl.ch/labs/lpbs/
Phone: +41789122090

Work experience

Ara-research, Tehran   **2016**

Researcher

- Building a scanning electron microscope.

Modaresan-e sharif (institute of education)   **2013 — 2017**

Editor

- Editing several books in mathematics and physics for the institute.
- Designing tests for preparation for master and doctoral nation-wide entrance exam.

Sharif University of Technology   **2016 — 2017**

A research into cosmic rays sources and detectors

- I and Mr Heydarizad have built a cloud chamber in professor Bahmanabadi's lab.

This is aired in Iran-national TV:
https://bit.ly/3nuLYG6

Qualifications

- JOURNAL ARTICLE AND CONFERENCES:

1. Optimizing checkpoint strategies based on first principles predicts experimental DNA damage checkpoint override times,
   Authors: A Sadeghi, R Dervey, V Gligorovski, SJ Rahi; under revision in nature physics;
   https://doi.org/10.1101/2020.08.14.251504
2. Multidimensional single-cell benchmarking of inducible promoters for precise dynamic control in budding yeast, under revision in nature communication.
   71
   Authors: V Gligorovski, A Sadeghi, SJ Rahi;
   https://doi.org/10.1101/2020.08.16.253310
3. YeaZ: A convolutional neural network for highly accurate, label-free

segmentation of yeast microscopy images, Authors: N Dietler, M Minder, V Gligorovski, AM Economou, DAHL Joly, A Sadeghi, Chun Hei Michael Chan, Mateusz Koziński, Martin Weigert, Anne-Florence Bitbol, Sahand Jamal Rahi;Nature Communications 11, 5723 (2020), https://doi.org/10.1038/s41467-020-19557-4

4. Emergent Weak Scale from Cosmological Evolution and Dimensional Transmutation, Authors: A Sadeghi, M Torabian; https://arxiv.org/abs/1512.02948

5. Crosstalk Suppression and High-Fidelity Measurement in 2-D Tunneling of Coupled Josephson Junctions, Authors: A Sadeghi, H Zandi, S Khorasani; *IEEE Transactions on Applied Superconductivity*; doi: 10.1109/TASC.2012.2193616.

- **COMPUTER SKILLS:**

    1. Programming Languages: C and C++, Quartus, AssemblyLanguage, and Python.

    2. Technical Software: Pspice, Codevision AVR, MatLab, AWR, and Mathematica.

    3. Other: Basics of machine learning, Microsoft Office, Math type, LaTeX…

- **QUALIFICATION EXAMS:**

    1. GRE Physics: 980/990
    2. GRE Quantitative: 170/170
    3. GRE Verbal: 144/170
    4. TOEFL: Reading 27,Listening 21,Speaking 22, Writing 23

- **HONORS AND AWARDS:**
    Ranked 73rd in nationwide entrance exam into bachelor of science among 319,259 (top 0.02%) students in 2008**. Ranked 13th** in nationwide entrance exam into master of science of around 13,000 students in 2013 and **ranked 3rd** in nationwide entrance exam into PhD of physics in 2015.

- **MAIN DUTIES DURING PhD:**

    1. Carried out molecular biology experiments, including DNA extraction, PCR, qPCR, molecular cloning, gel electrophoresis, making DNA constructs, …
    2. Fluorescence-activated cell sorting, including SONY-SH800S, and Attune NxT.
    3. Microscopy, including fluorescence microscopy (Nikon Ti2).
    4. Microfluidic (studying the dynamics of gene expression in budding yeast cells).

Education

PhD in Biophysics   01/08/2018 — 09/07/2021

École polytechnique fédérale de Lausanne (EPFL)

Thesis title: Principles of checkpoint override

72

MSc in Physics   22/08/2013 — 22/08/2015

Sharif University of Technology

Thesis title: Emergence of the Electroweak Scale via Cosmic Relation and Quantum Corrections.

BSc in Electerical Engineering   **22/08/2008 — 22/08/2013**

Sharif University of Technology

Thesis title: A research into high temperature superconductivity.

Interests

Music, Reading, Biking

73